AF3 Modeling of DNA Nanomotifs: Is it reliable?

Mauricio Cortes Jr,[#] Xindi Sun,[#] Anusha, Emile Joseph Batchelder-Schwab, Jinyue Li, Naseem siraj Koomullam kattil, Rishab Jampana, Yuchen Zhang, Yuntian Bai, and Chengde Mao*

Department of Chemistry, Purdue University, West Lafayette, IN 47907, USA

[#] contribute equally

Email: mao@purdue.edu

Supplementary Information

AF3 modeling. All modeling was performed using the AF3 server at https://golgi.sandbox.google.com/. All structures have been modeling separately in the presence and in the absence of 10 sodium ions (Na^+) and 10 magnesium ions (Mg^{2+}). For most of the structures, the resulting structures from the two different conditions are the same. All data presented, except Fig 5c, are modeled in the presence of 10 sodium ions (Na^+) and 10 magnesium ions (Mg^{2+}). The data in Fig. 5c are from a modeling without any additional cations.

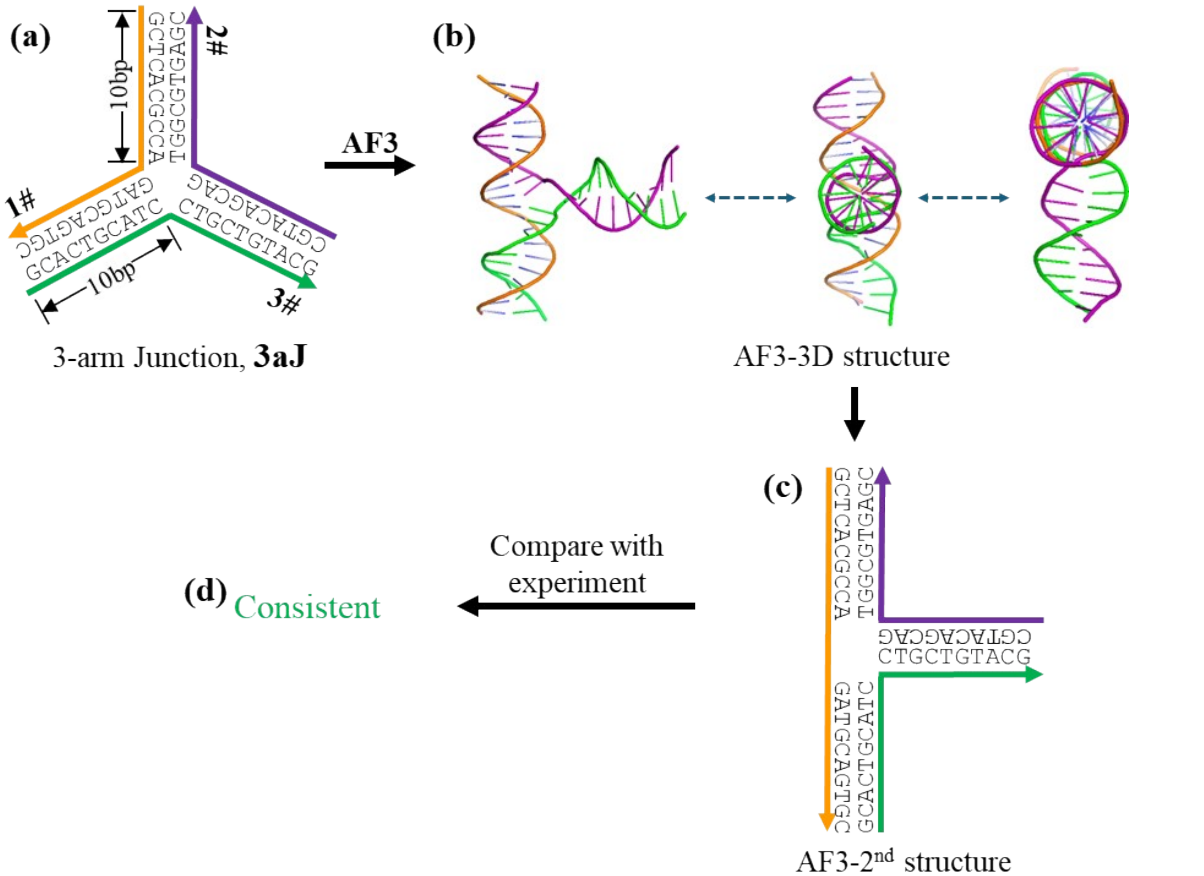

Figure S1. AF3 modeling of a DNA 3-arm junction, 3aJ. (a) The sequence design of the 3aJ. (b) AF3-predicted 3D model of the 3aJ in three orthogonal views. (c) The corresponding secondary (2nd) structure of the 3D structure. (d) Comparison between the AF3 model and experimentally observed 2nd structure.

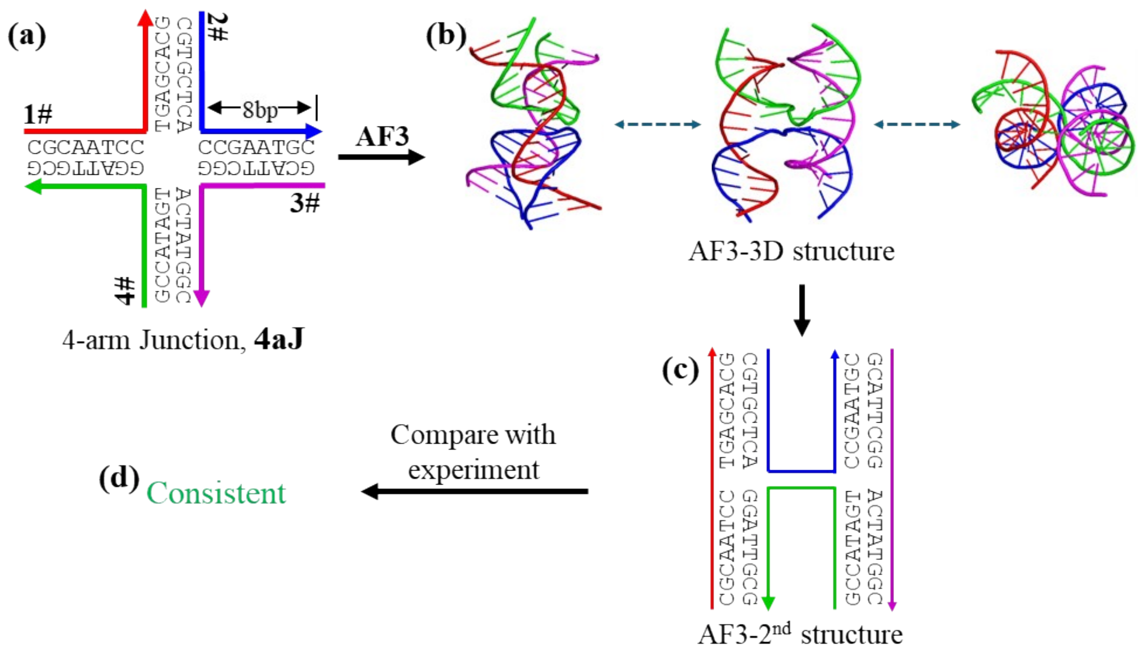

Figure S2. AF3 modeling of a DNA 4-arm junction, 4aJ. (a) The sequence design of the 4aJ. (b) AF3-predicted 3D model of the 4aJ in three orthogonal views. (c) The corresponding secondary (2nd) structure of the 3D structure. (d) Comparison between the AF3 model and experimentally observed 2nd structure.

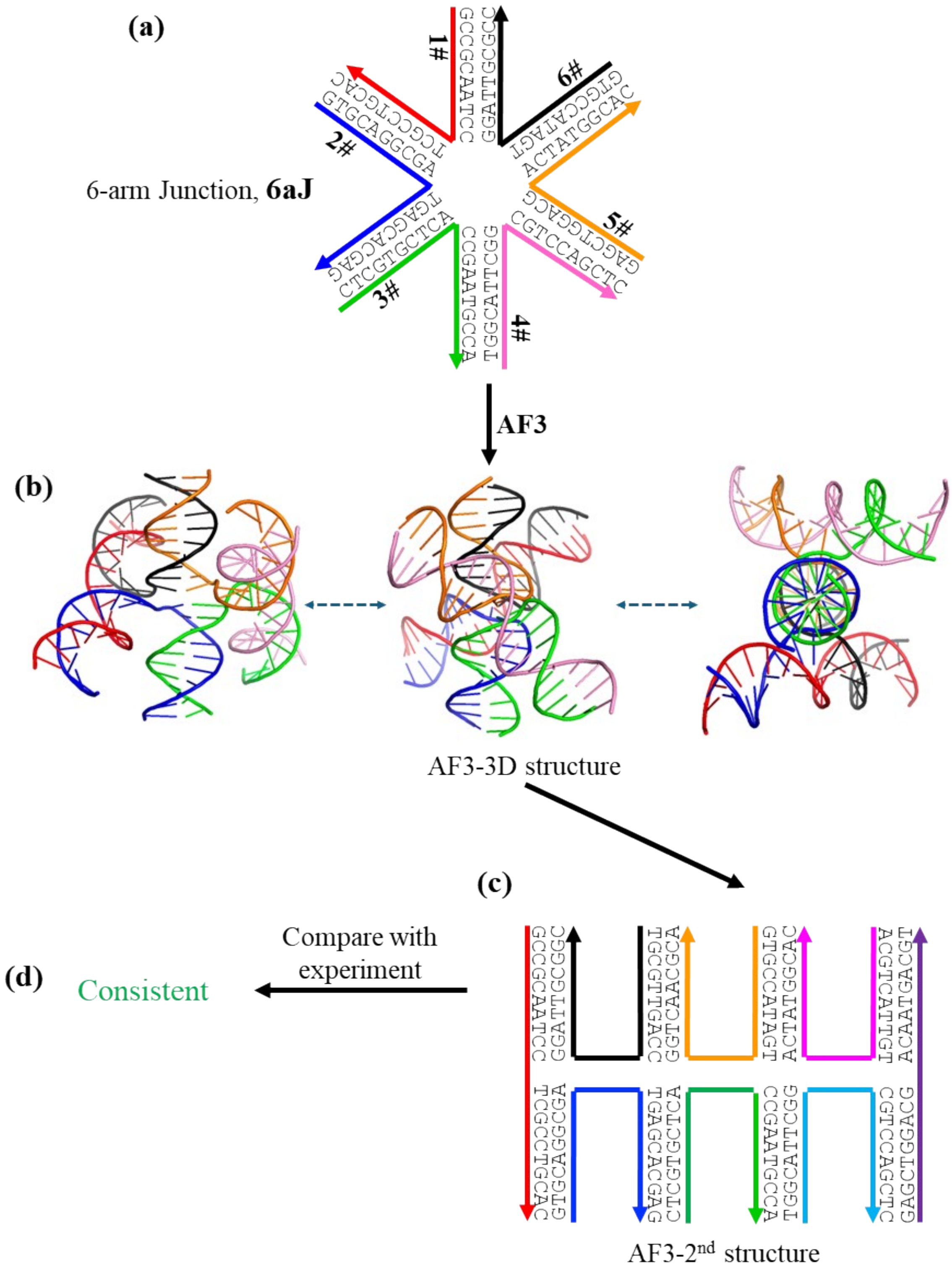

Figure S3. AF3 modeling of a DNA 6-arm junction, 6aJ. (a) The sequence design of the 6aJ. (b) AF3-predicted 3D model of the 6aJ in three orthogonal views. (c) The corresponding secondary (2nd) structure of the 3D structure. (d) Comparison between the AF3 model and experimentally observed 2nd structure.

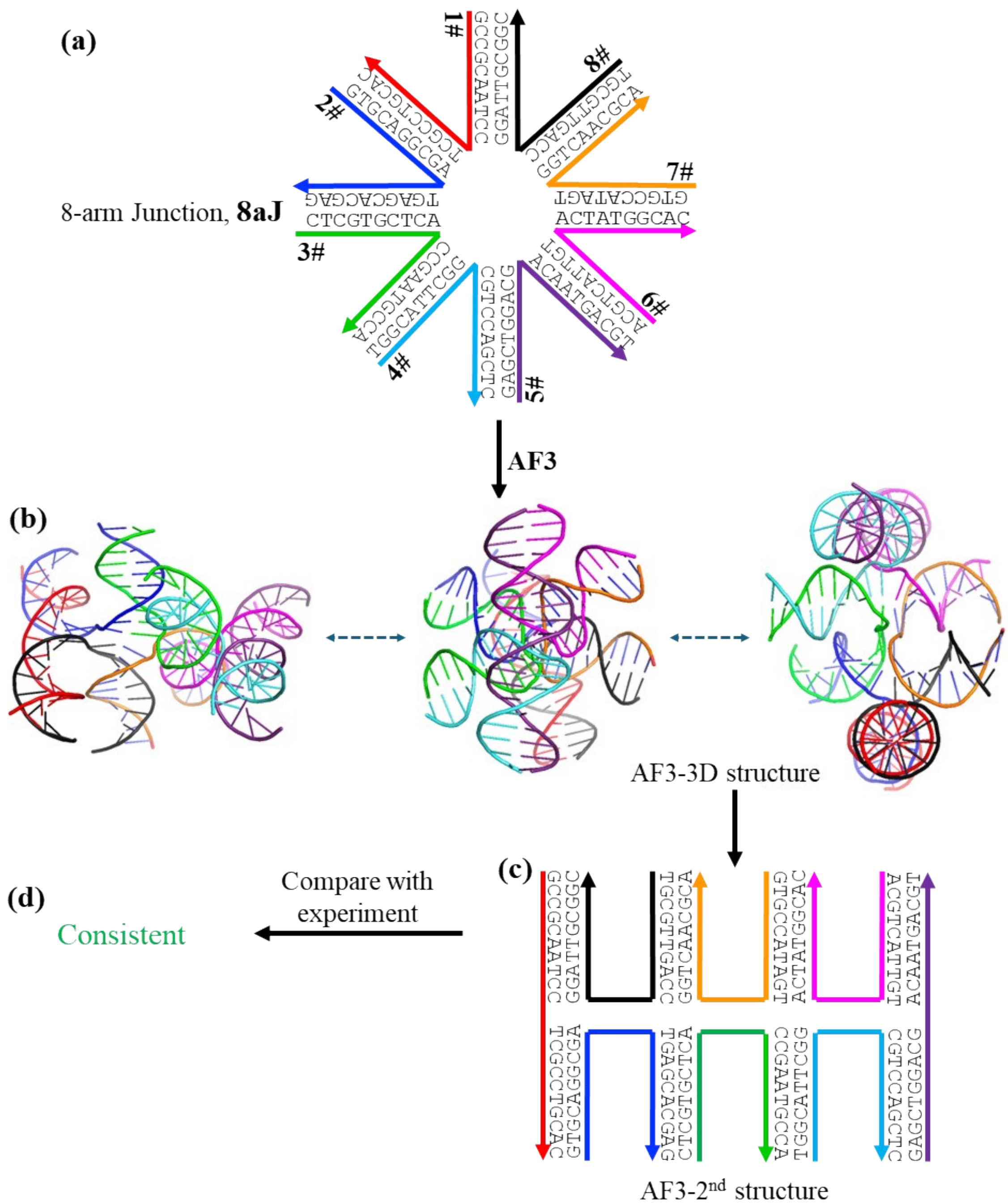

Figure S4. AF3 modeling of a DNA 8-arm junction, 8aJ. (a) The sequence design of the 8aJ. (b) AF3-predicted 3D model of the 8aJ in three orthogonal views. (c) The corresponding secondary (2nd) structure of the 3D structure. (d) Comparison between the AF3 model and experimentally observed 2nd structure.

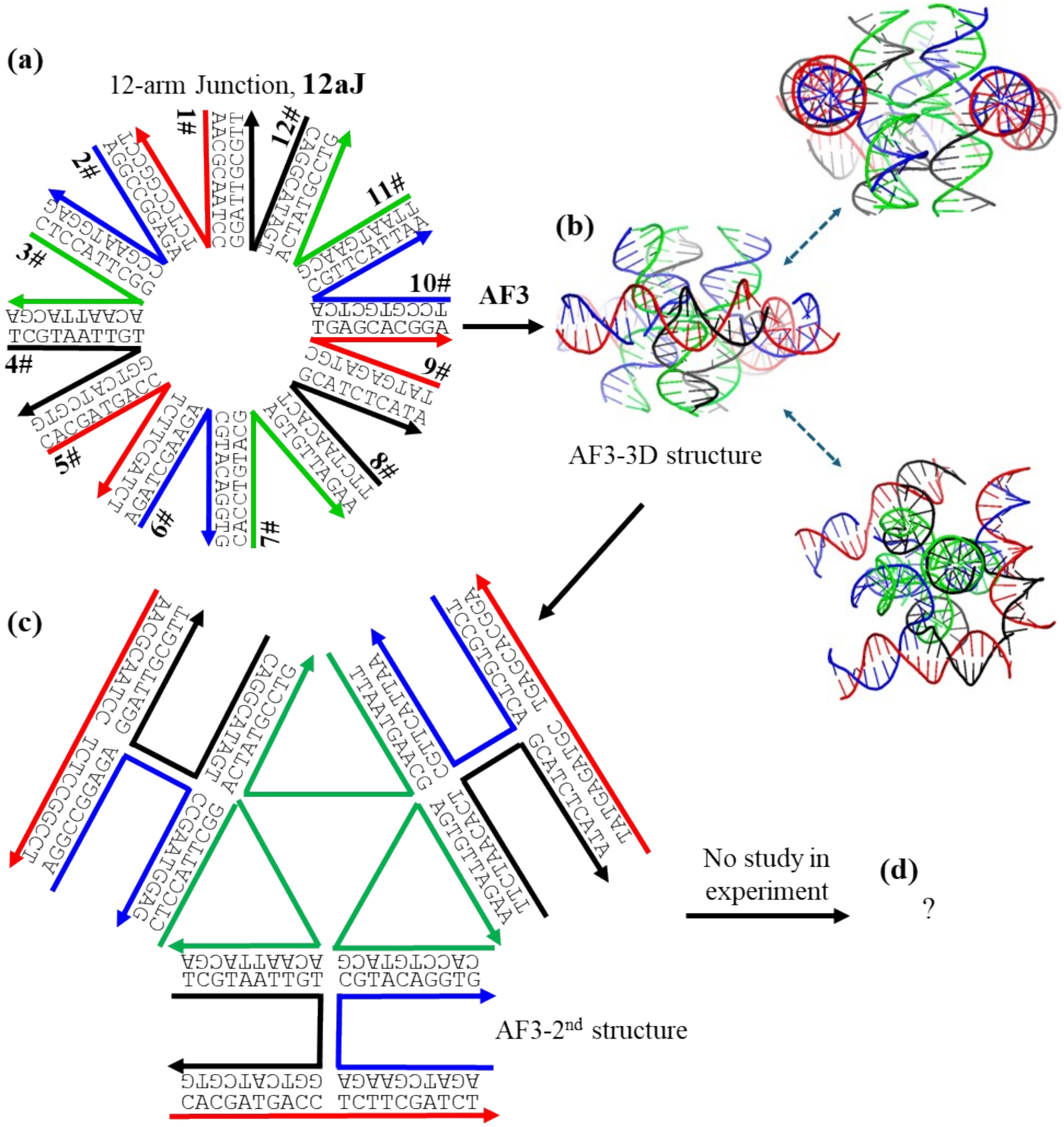

Figure S5. AF3 modeling of a DNA 12-arm junction, 12aJ. (a) The sequence design of a 12aJ. (b) AF3-predicted 3D model of the 12aJ in three orthogonal views. (c) The corresponding secondary (2nd) structure of the 3D structure. (d) Comparison between the AF3 model and experimentally observed 2nd structure. As there no experimental data available, no conclusion can be drawn.

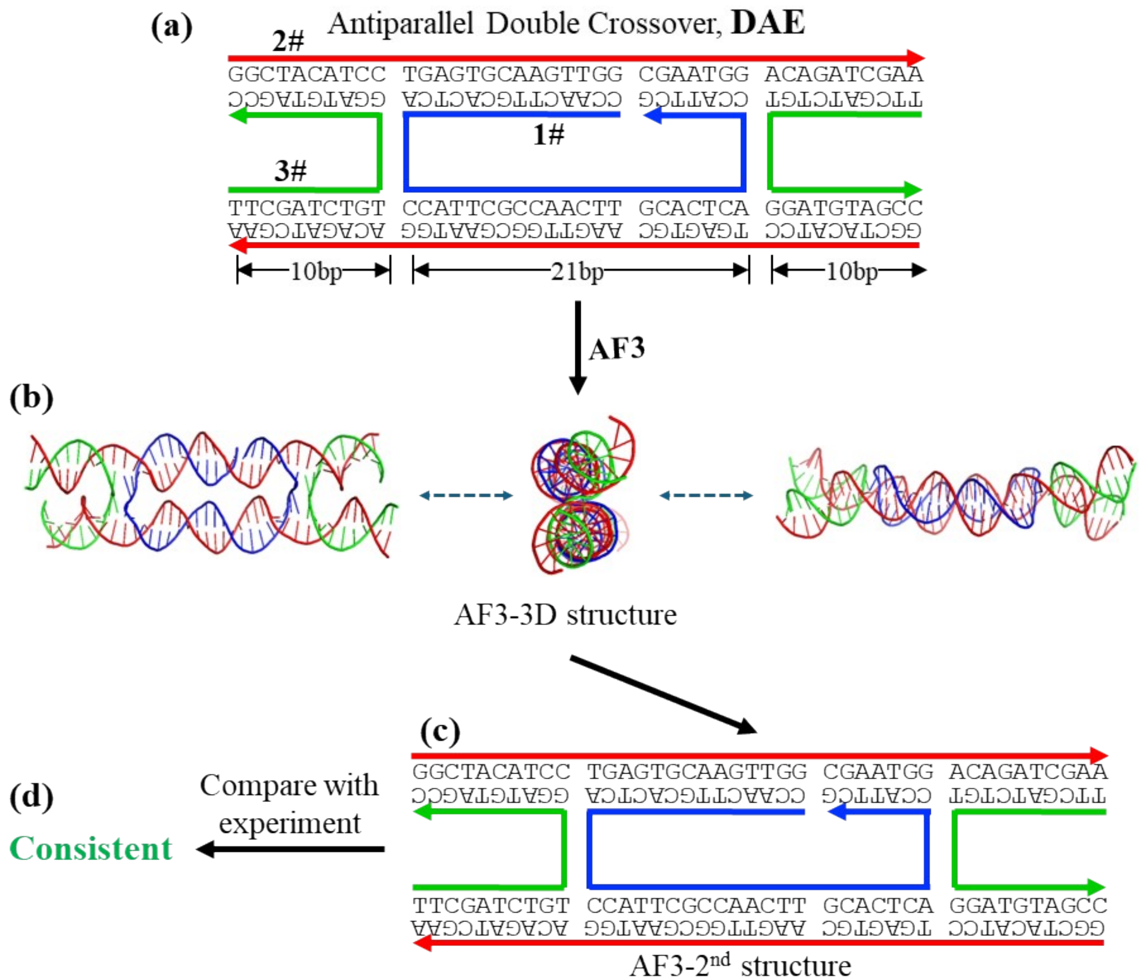

Figure S6. AF3 modeling of a DNA antiparallel double crossover, DAE (a) The sequence design of the DAE. (b) AF3-predicted 3D model of the DAE in three orthogonal views. (c) The corresponding secondary (2nd) structure of the 3D structure. (d) Comparison between the AF3 model and experimentally observed 2nd structure.

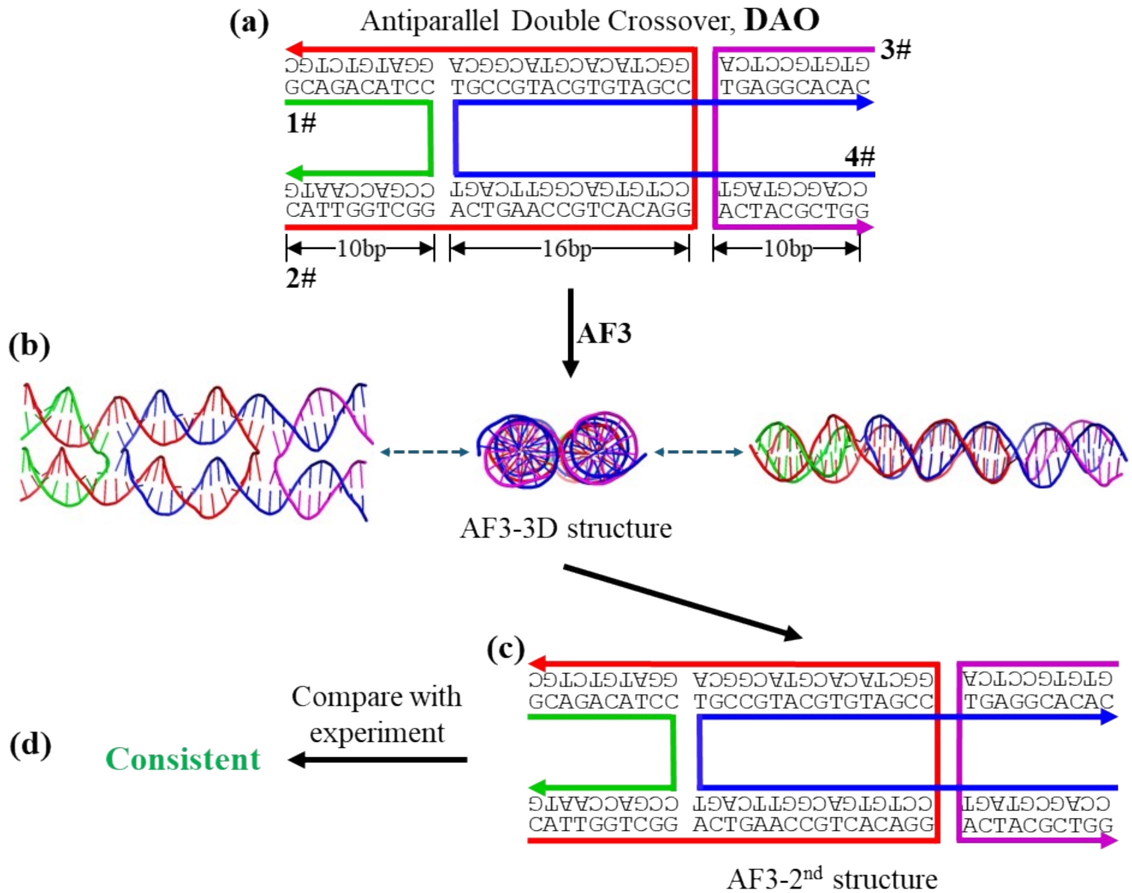

Figure S7. AF3 modeling of a DNA antiparallel double crossover, DAO. (a) The sequence design of the DAO. (b) AF3-predicted 3D model of the DAOin three orthogonal views. (c) The corresponding secondary (2nd) structure of the 3D structure. (d) Comparison between the AF3 model and experimentally observed 2nd structure.

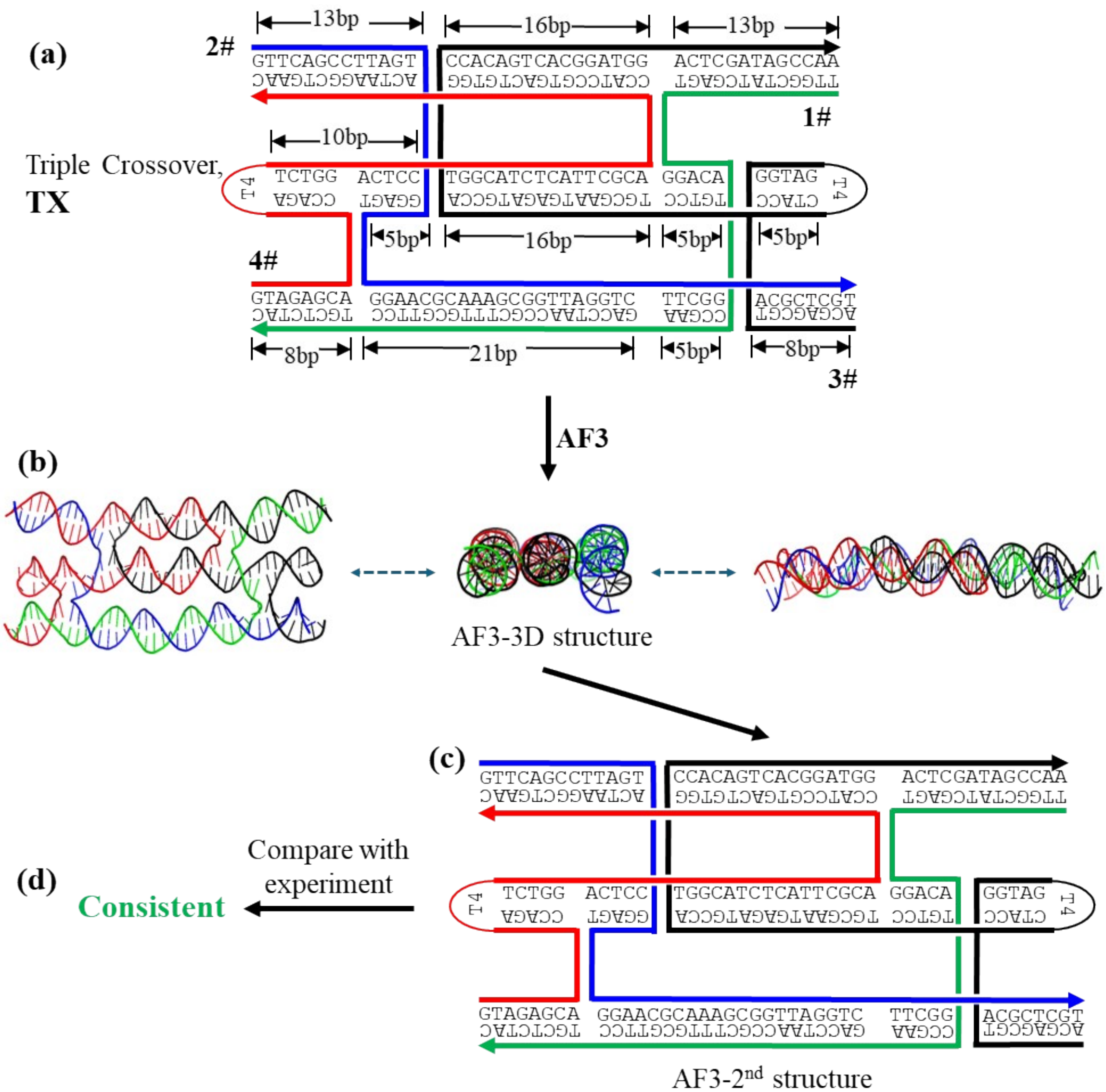

Figure S8. AF3 modeling of a DNA triple crossover, TX. (a) The sequence design of the TX. (b) AF3-predicted 3D model of the TX in three orthogonal views. (c) The corresponding secondary (2nd) structure of the 3D structure. (d) Comparison between the AF3 model and experimentally observed 2nd structure.

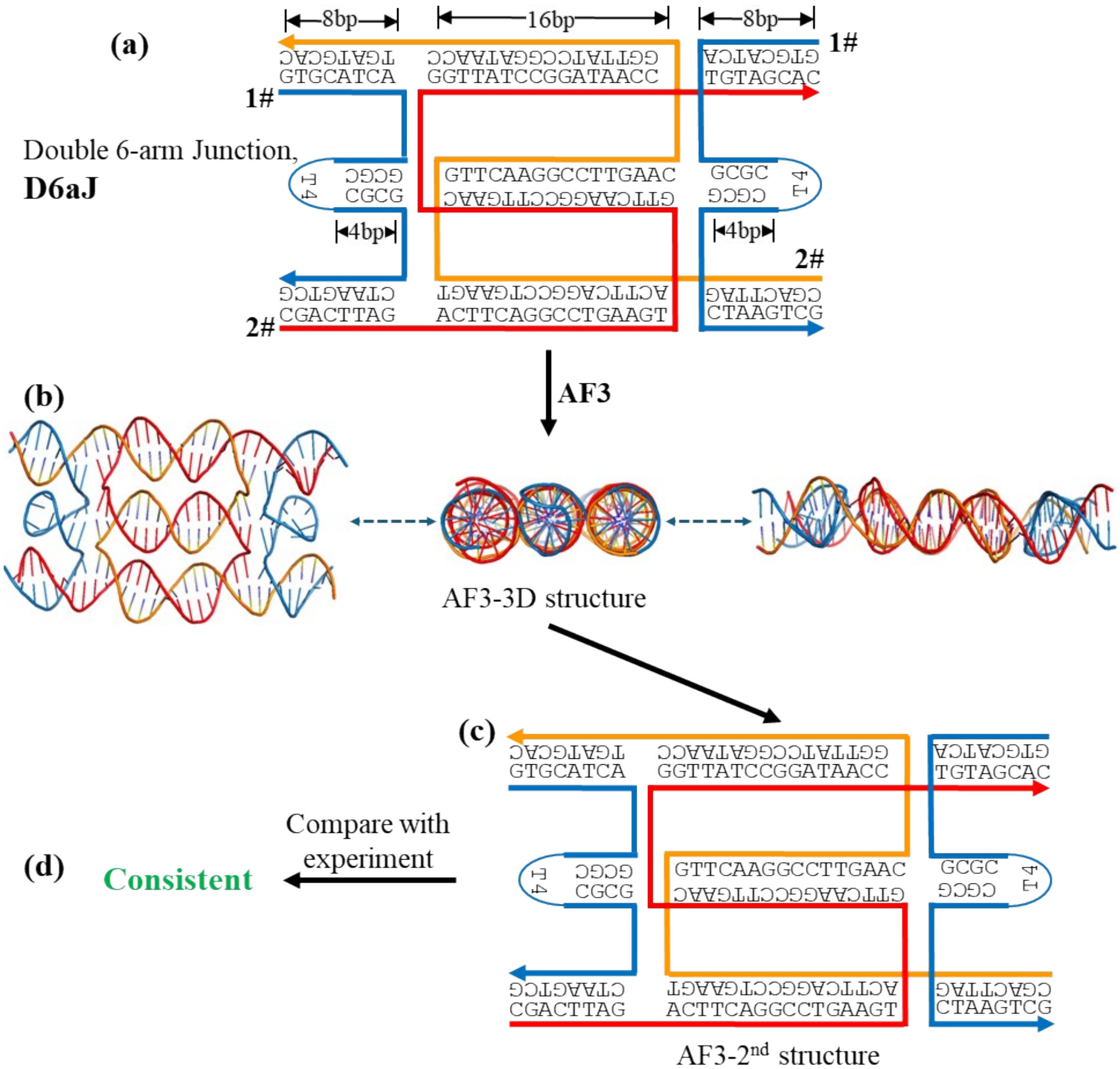

Figure S9. AF3 modeling of a Double 6-arm Junction, D6aJ. (a) The sequence design of the D6aJ. (b) AF3-predicted 3D model of the D6aJ in three orthogonal views. (c) The corresponding secondary (2nd) structure of the 3D structure. (d) Comparison between the AF3 model and experimentally observed 2nd structure.

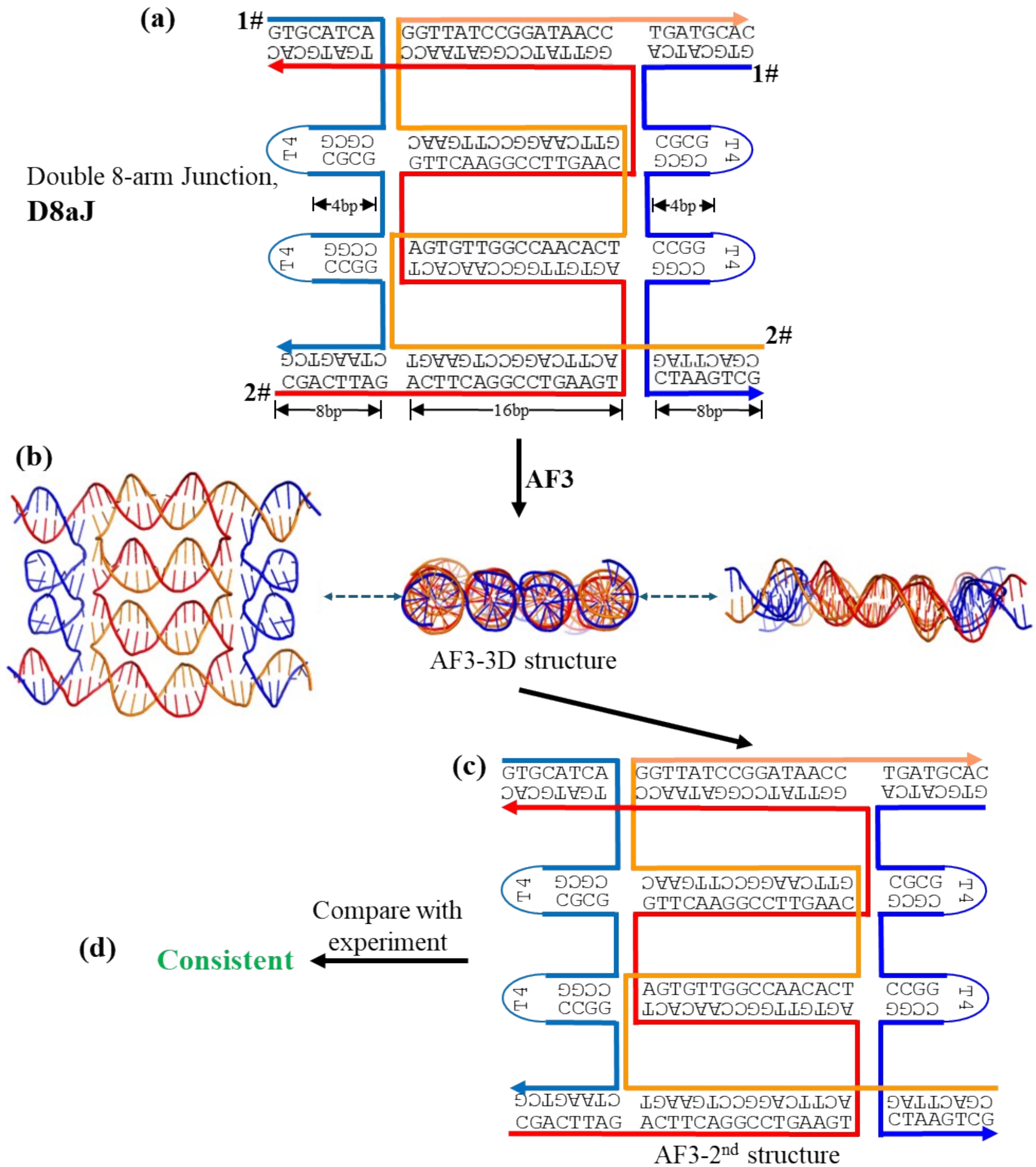

Figure S10. AF3 modeling of a Double 8-arm Junction, D8aJ. (a) The sequence design of the D8aJ. (b) AF3-predicted 3D model of the D8aJ in three orthogonal views. (c) The corresponding secondary (2nd) structure of the 3D structure. (d) Comparison between the AF3 model and experimentally observed 2nd structure.

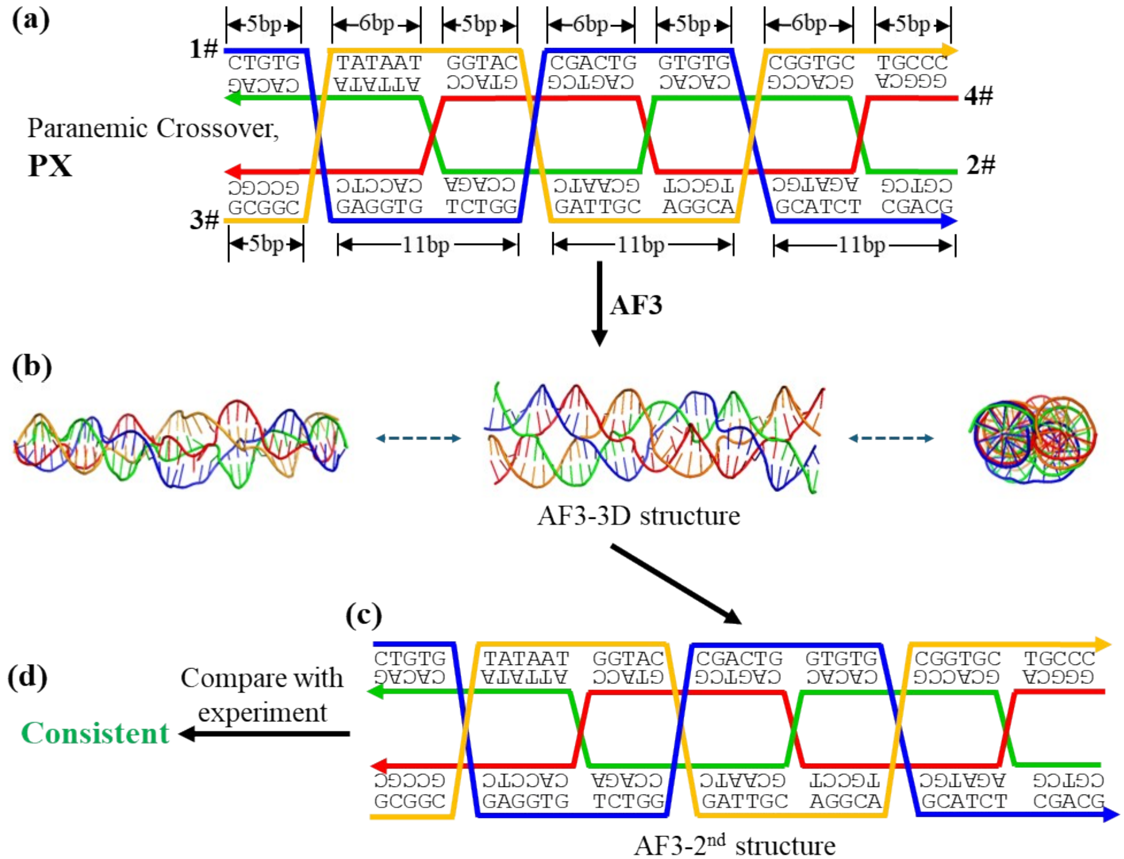

Figure S11. AF3 modeling of a DNA paranemic crossover, PX. (a) The sequence design of the PX. (b) AF3-predicted 3D model of the PX in three orthogonal views. (c) The corresponding secondary (2nd) structure of the 3D structure. (d) Comparison between the AF3 model and experimentally observed 2nd structure.

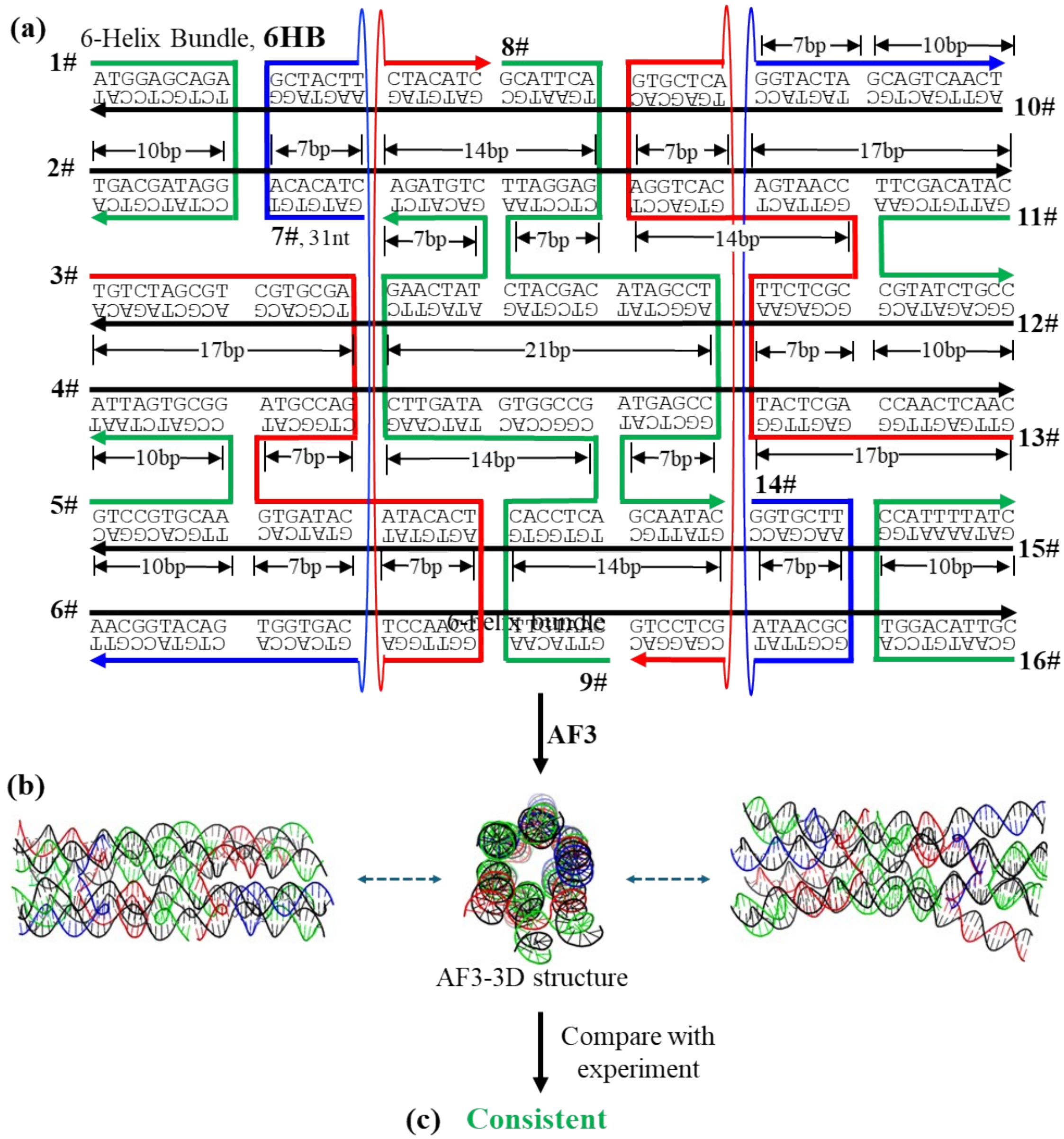

Figure S12. AF3 modeling of a DNA 6-helix bundle, 6HB. (a) The sequence design of the 6HB. (b) AF3-predicted 3D model of the 6HB in three orthogonal views. (c) The corresponding secondary (2nd) structure of the 3D structure. (d) Comparison between the AF3 model and experimentally observed 2nd structure.

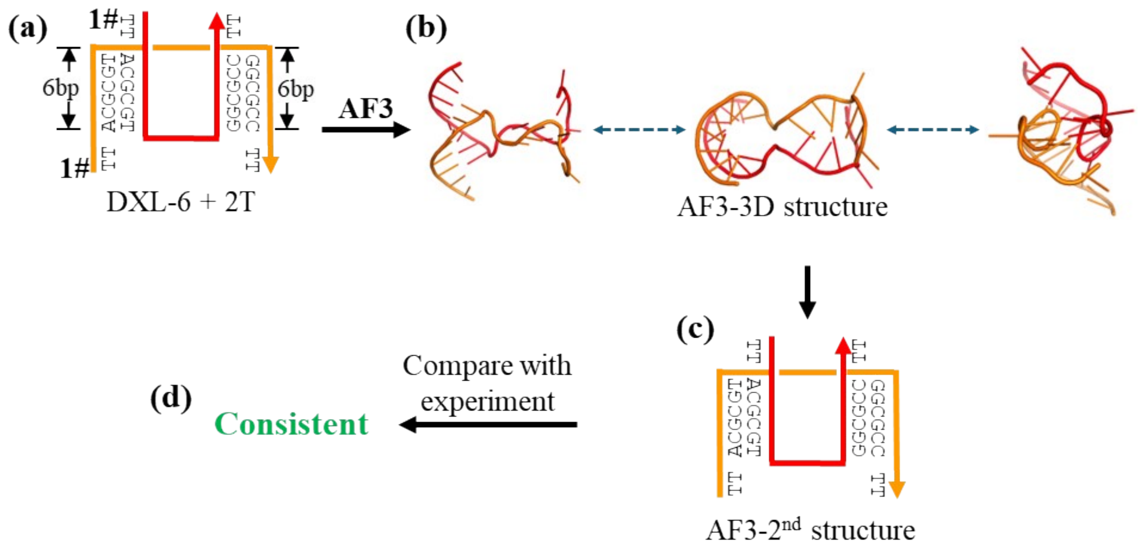

Figure S13. AF3 modeling of a small DNA double crossover-like motif with 6-base pair (bp) separation, DXL-6. (a) The sequence design of the small DXL-6. (b) AF3-predicted 3D model of the DXL-6 in three orthogonal views. (c) The corresponding secondary (2nd) structure of the 3D structure. (d) Comparison between the AF3 model and experimentally observed 2nd structure.

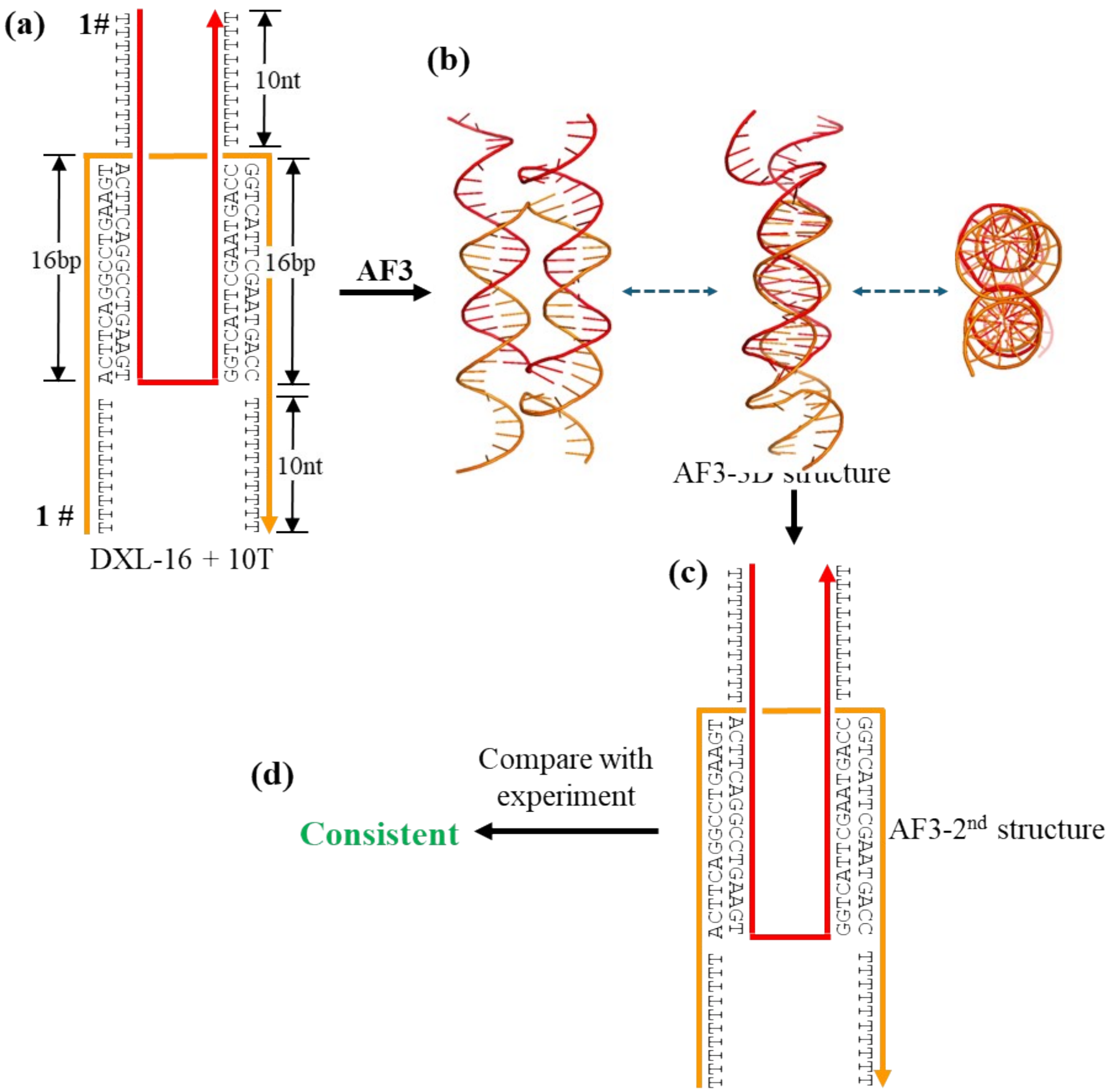

Figure S14. AF3 modeling of a large DNA double crossover-like motif with 16-bp separation, DXL-16. (a) The sequence design of the large DXL-16. (b) AF3-predicted 3D model of the DXL-16 in three orthogonal views. (c) The corresponding secondary (2nd) structure of the 3D structure. (d) Comparison between the AF3 model and experimentally observed 2nd structure.

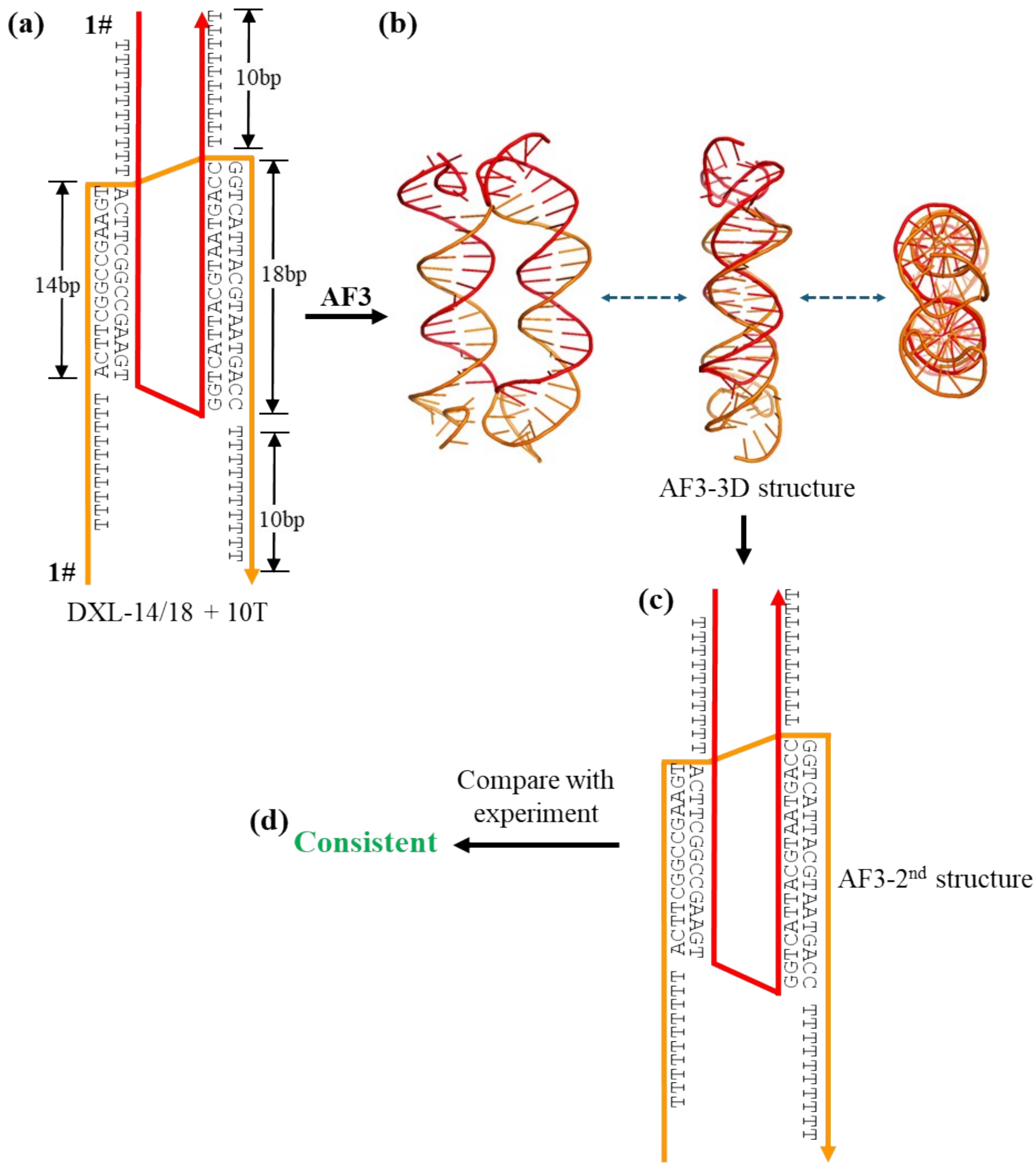

Figure S15. AF3 modeling of an asymmetric DNA double crossover-like motif, DXL-14/18. (a) The sequence design of the asymmetric DXL. (b) AF3-predicted 3D model of the asymmetric DXL in three orthogonal views. *Note the overall bending of the asymmetric DXL from the long helical domain toward the short helical domain.* (c) The corresponding secondary (2nd) structure of the 3D structure. (d) Comparison between the AF3 model and experimentally observed 2nd structure.

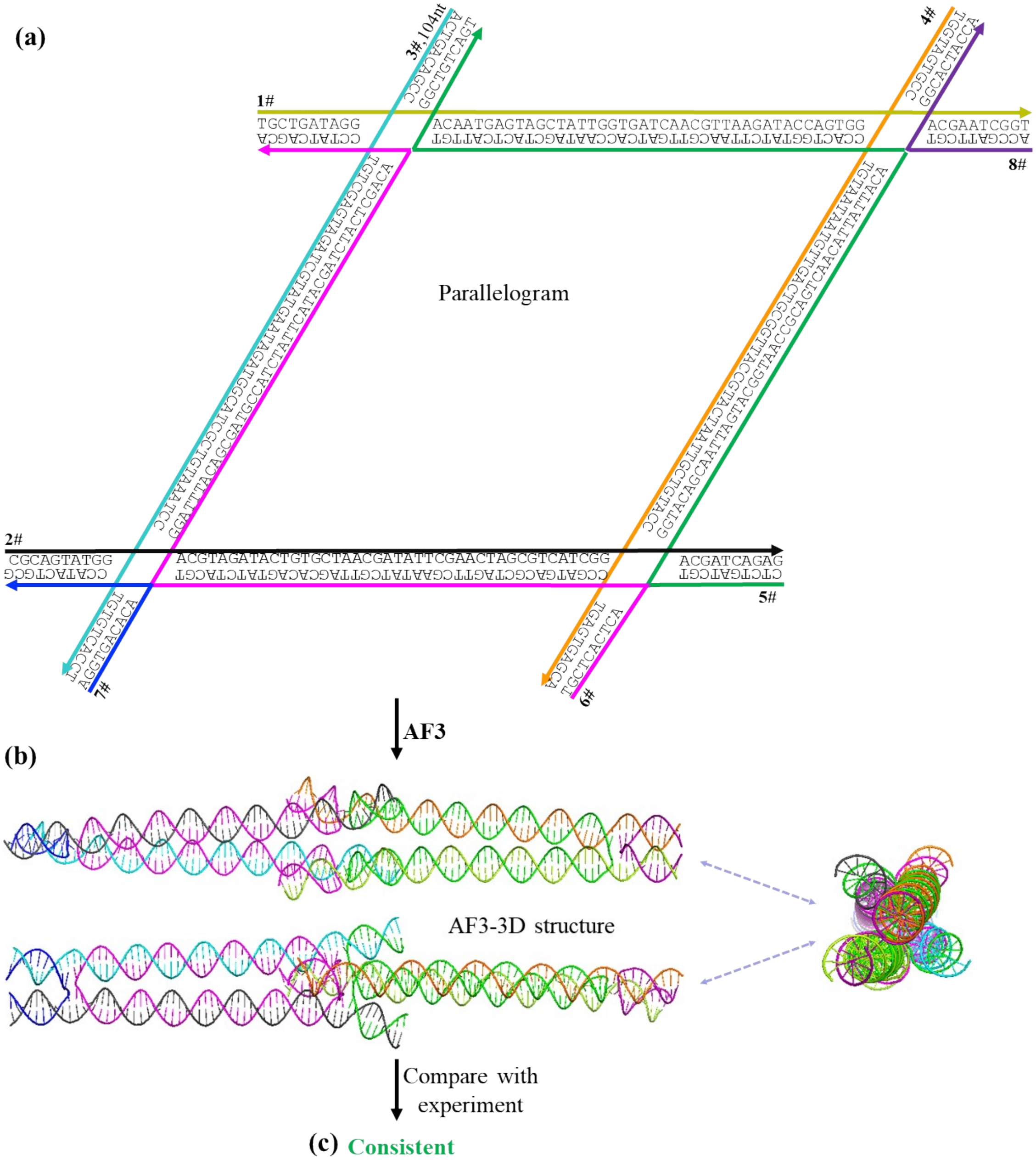

Figure S16. AF3 modeling of a DNA parallelogram. (a) The sequence design of the parallelogram. (b) AF3-predicted 3D model of the parallelogram in three orthogonal views. (c) Comparison between the AF3 model and experimentally observed 2nd structure.

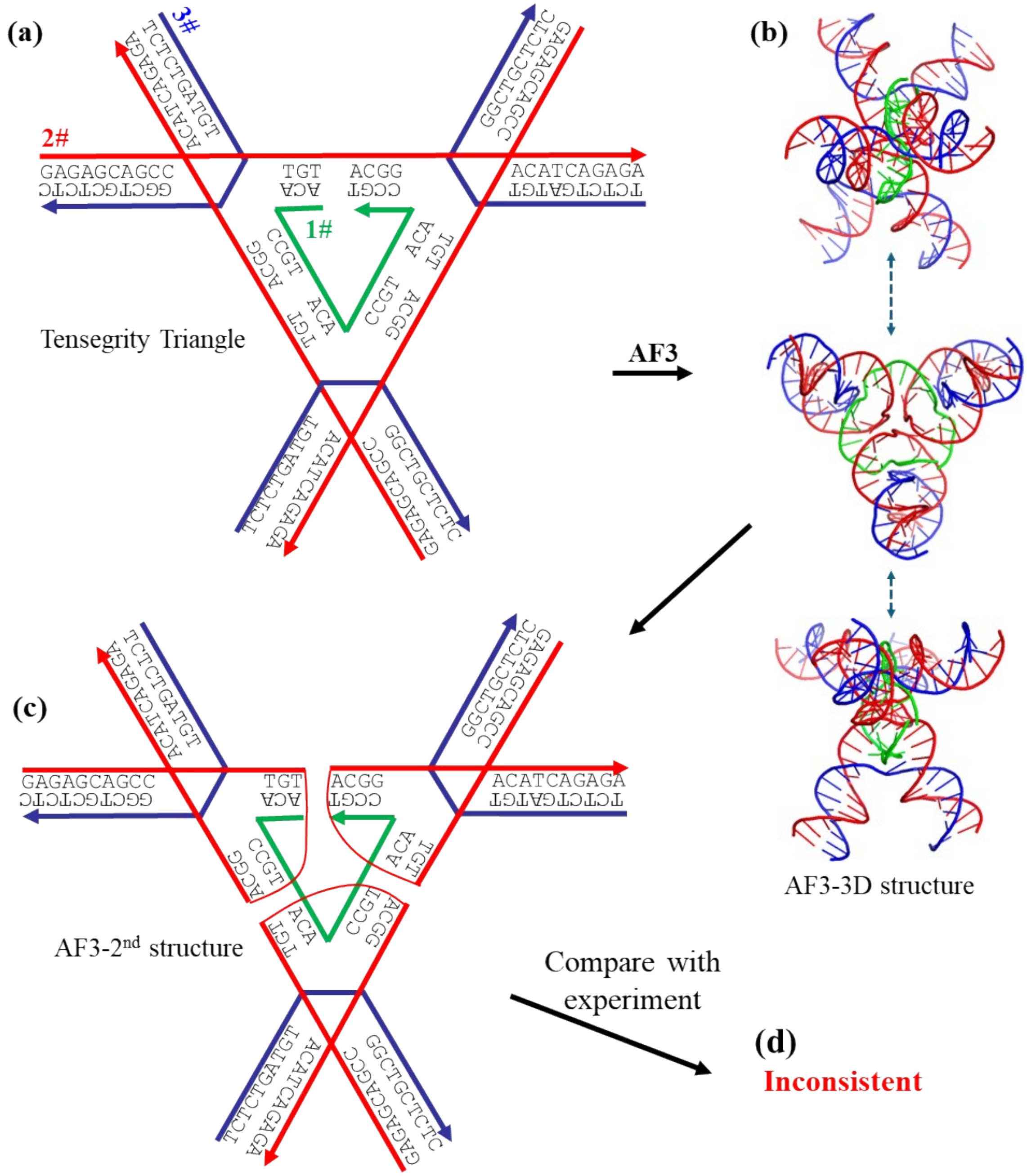

Figure S17. AF3 modeling of a symmetric DNA tensegrity triangle. (a) The sequence design of the triangle. (b) AF3-predicted 3D model of the triangle in three orthogonal views. (c) The corresponding secondary (2nd) structure of the 3D structure. *Note that the red strands crossover from one duplex to another duplex instead of being continuously on one duplex*. (d) Comparison between the AF3 model and experimentally observed 2nd structure.

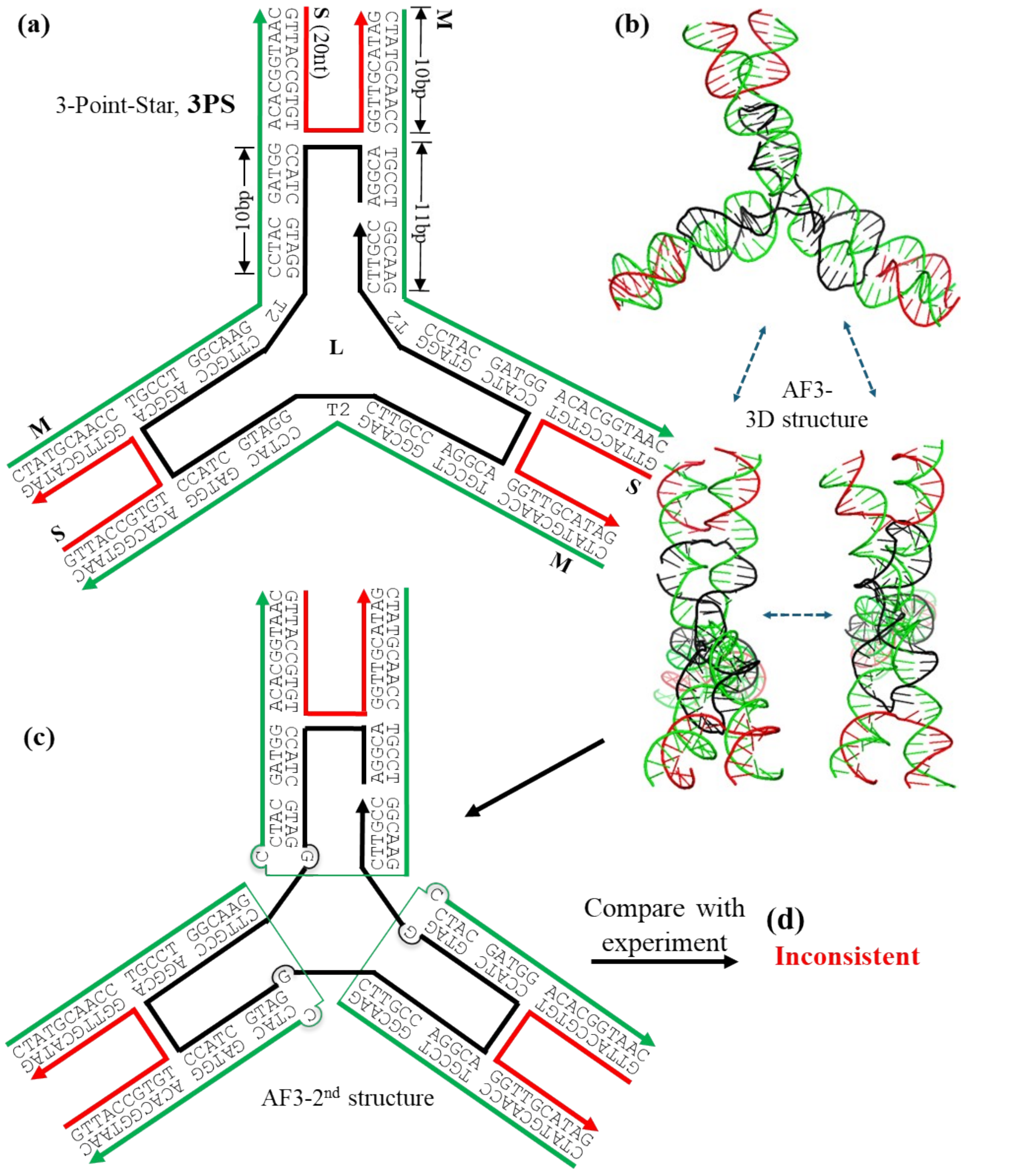

Figure S18. AF3 modeling of a symmetric DNA 3-point-star motif, s3PS. (a) The sequence design of the s3PS. Note that there is a 3-fold rotational symmetry at the motif center. All green strands are identical to each other and all red strands are identical to each other. (b) AF3-predicted 3D model of the s3PS in three orthogonal views. (c) The corresponding secondary (2nd) structure of the 3D structure. *Note that the green strands make U-turns in the same branch instead of crossing from one branch to another branch at the 3PS center*. (d) Comparison between the AF3 model and experimentally observed 2nd structure.

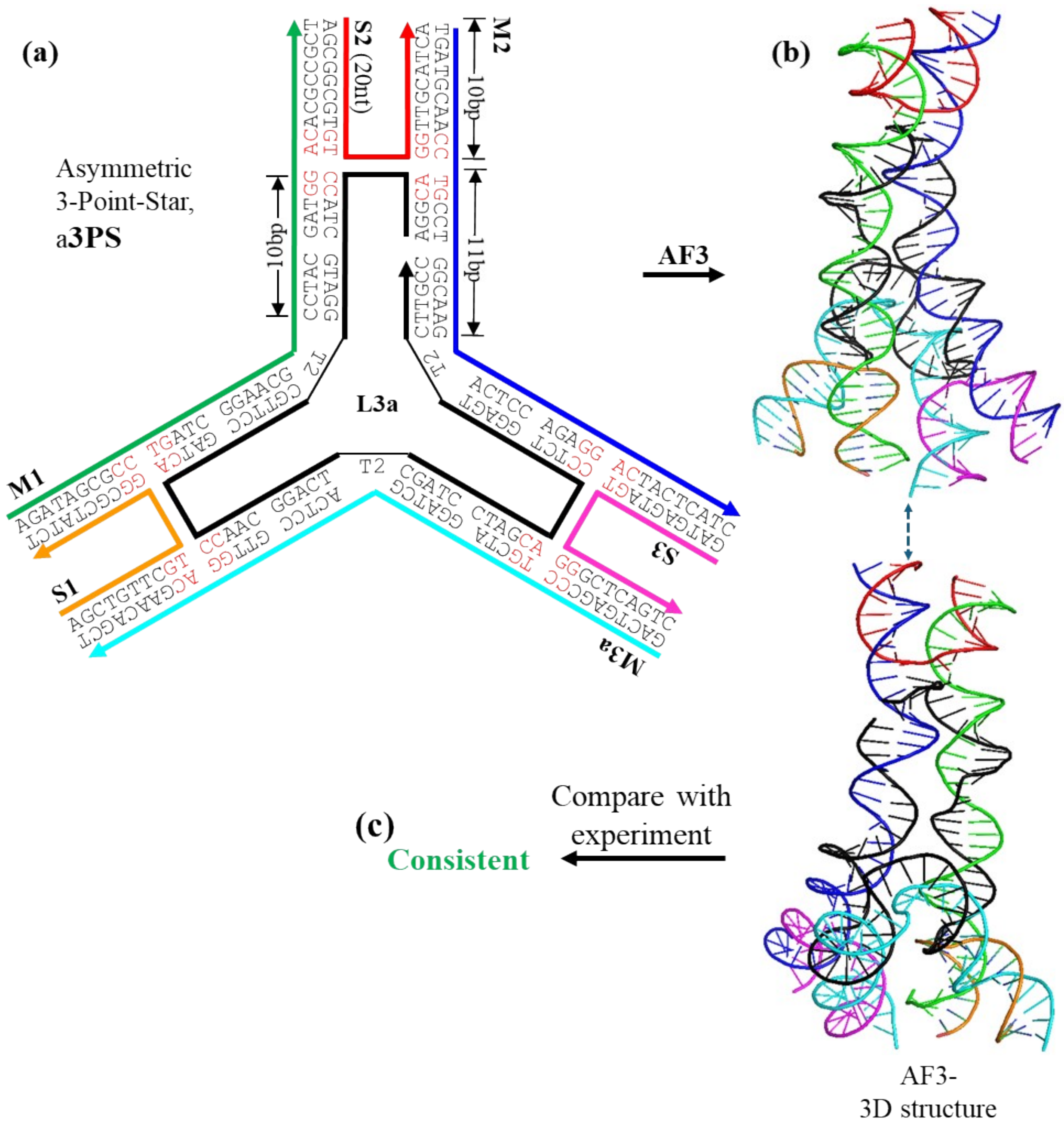

Figure S19. AF3 modeling of an asymmetric DNA 3-point-star motif, a3PS. (a) The sequence design of the a3PS. Note that there is no 3-fold rotational symmetry for this motif; thus, all strands are unique. (b) AF3-predicted 3D model of the a3PS in two orthogonal views. (c) Comparison between the AF3 model and experimentally observed 2nd structure.

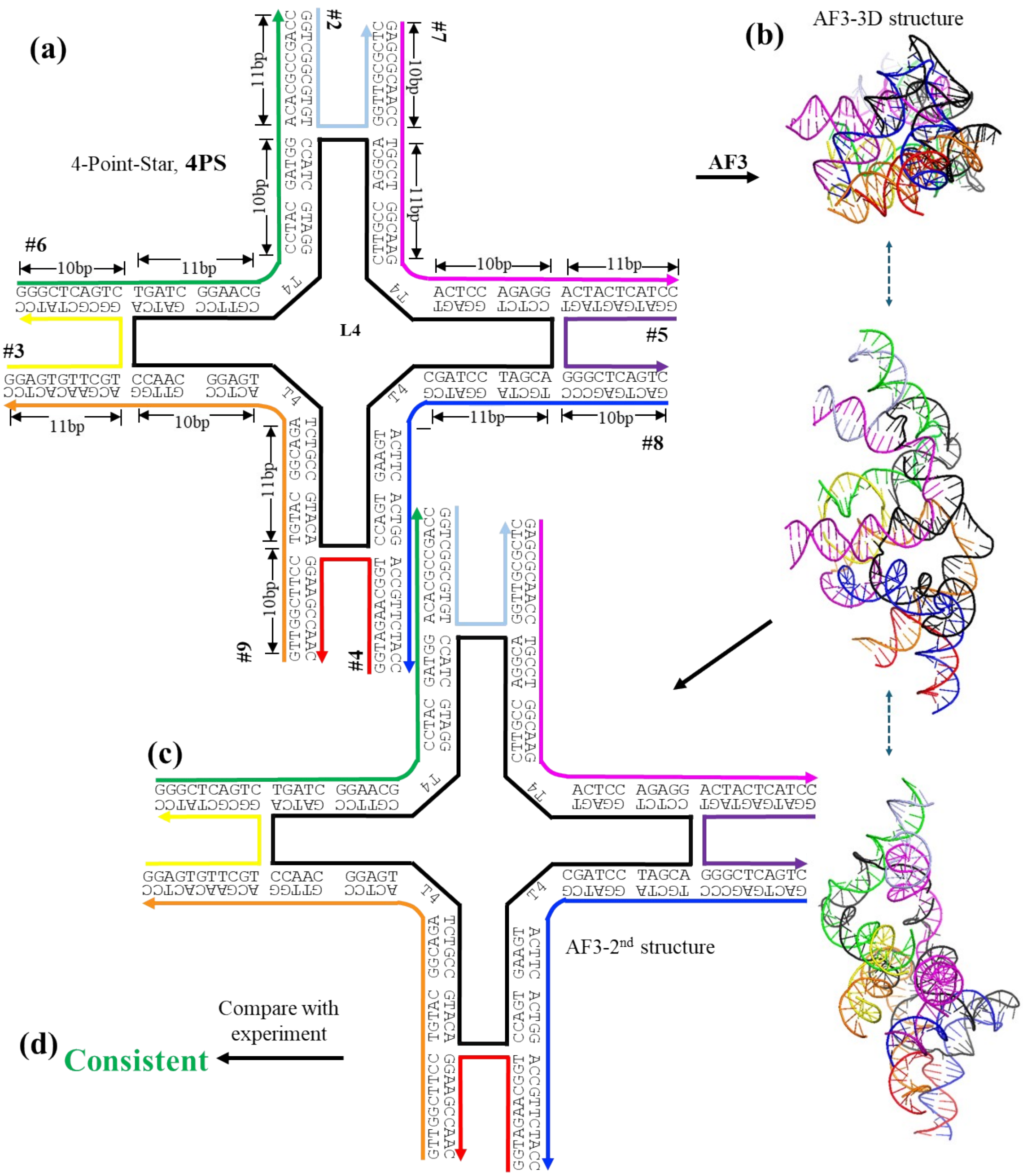

Figure S20. AF3 modeling of a symmetric DNA 4-point-star motif, s4PS. (a) The sequence design of the 4PS. Note that there is a 4-fold rotational symmetry at the motif center. All green strands are identical to each other and all red strands are identical to each other. (b) AF3-predicted 3D model of the s4PS in three orthogonal views. (c) The corresponding secondary (2nd) structure of the 3D structure. (d) Comparison between the AF3 model and experimentally observed 2nd structure.

(a)

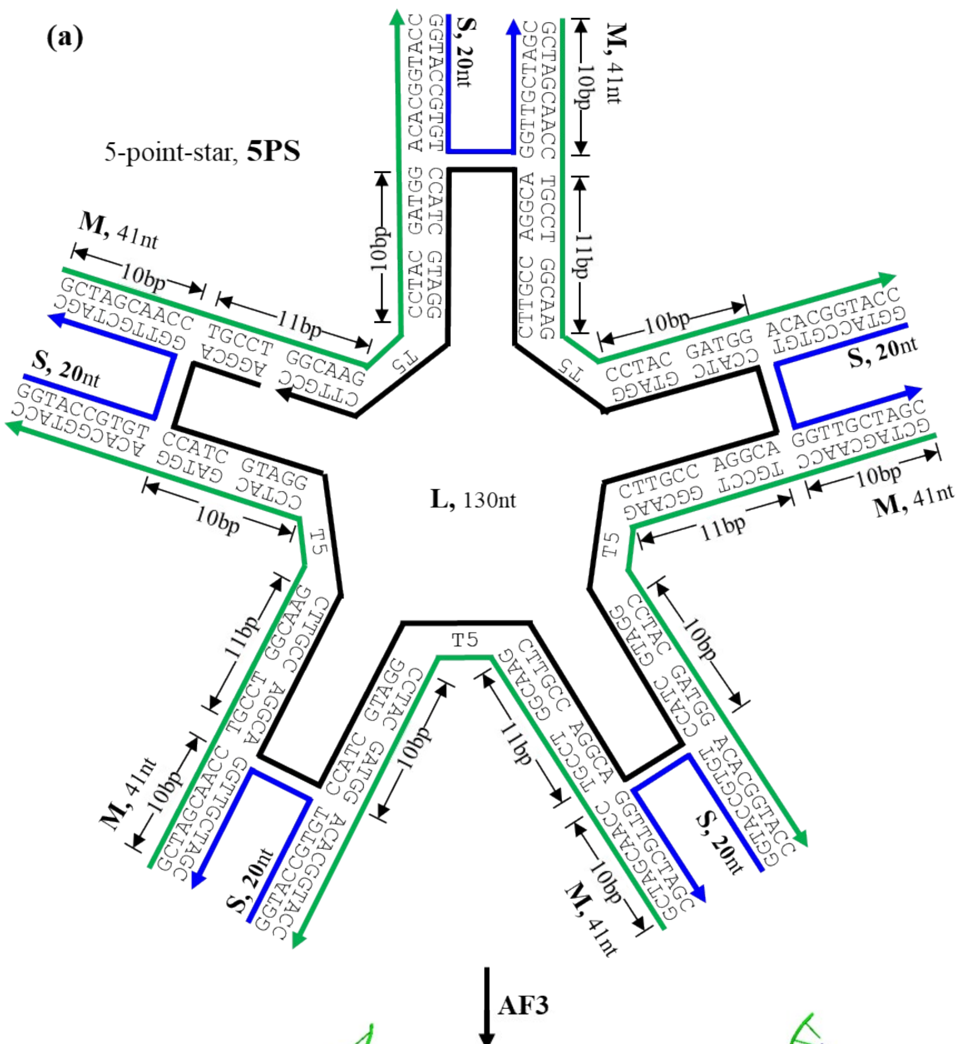

(b)

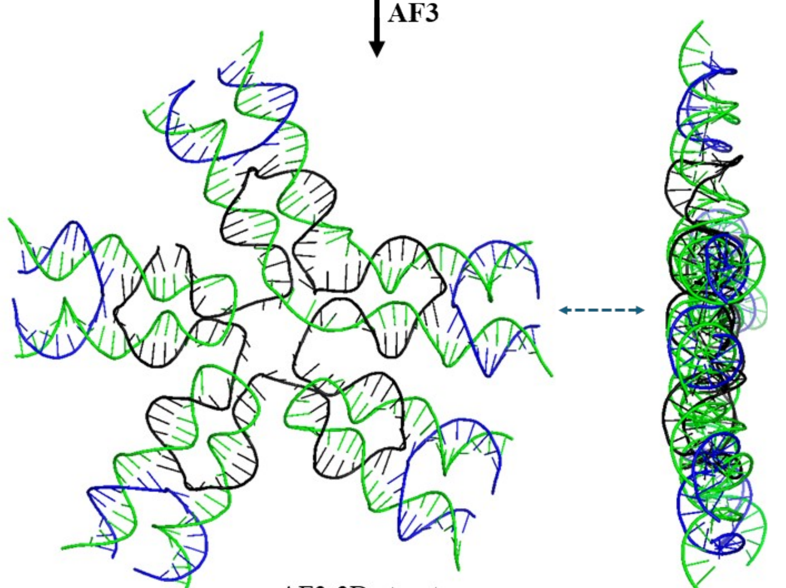

AF3-3D structure

continue…

(c)

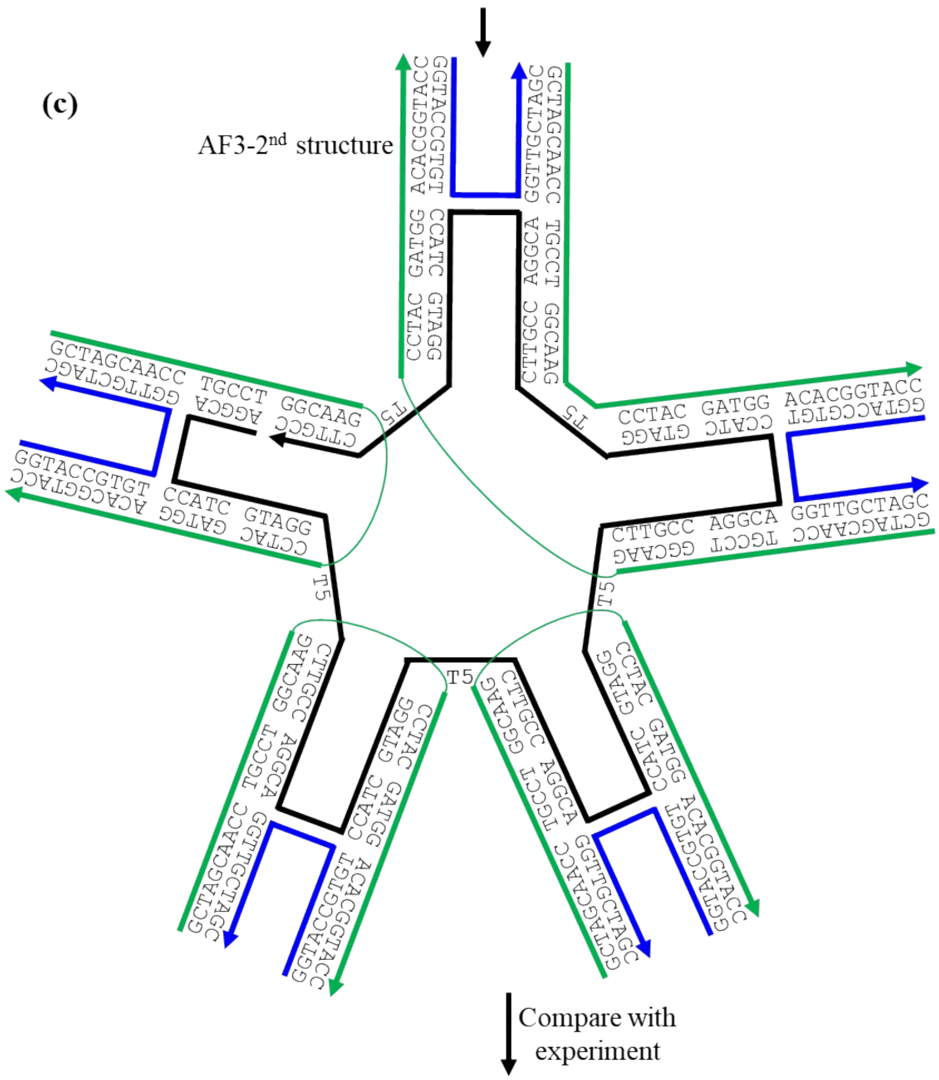

(d) **Inconsistent**

Figure S21. AF3 modeling of a symmetric DNA 5-point-star motif, s5PS. (a) The sequence design of the 5PS. Note that there is a 5-fold rotational symmetry at the motif center. All green strands are identical to each other and all red strands are identical to each other. (b) AF3-predicted 3D model of the s5PS in two orthogonal views. (c) The corresponding secondary (2nd) structure of the 3D structure. *Note that some of the green strands make U-turns in the same branch instead of crossing from one branch to another branch at the motif center.* (d) Comparison between the AF3 model and experimentally observed 2nd structure.

(a)

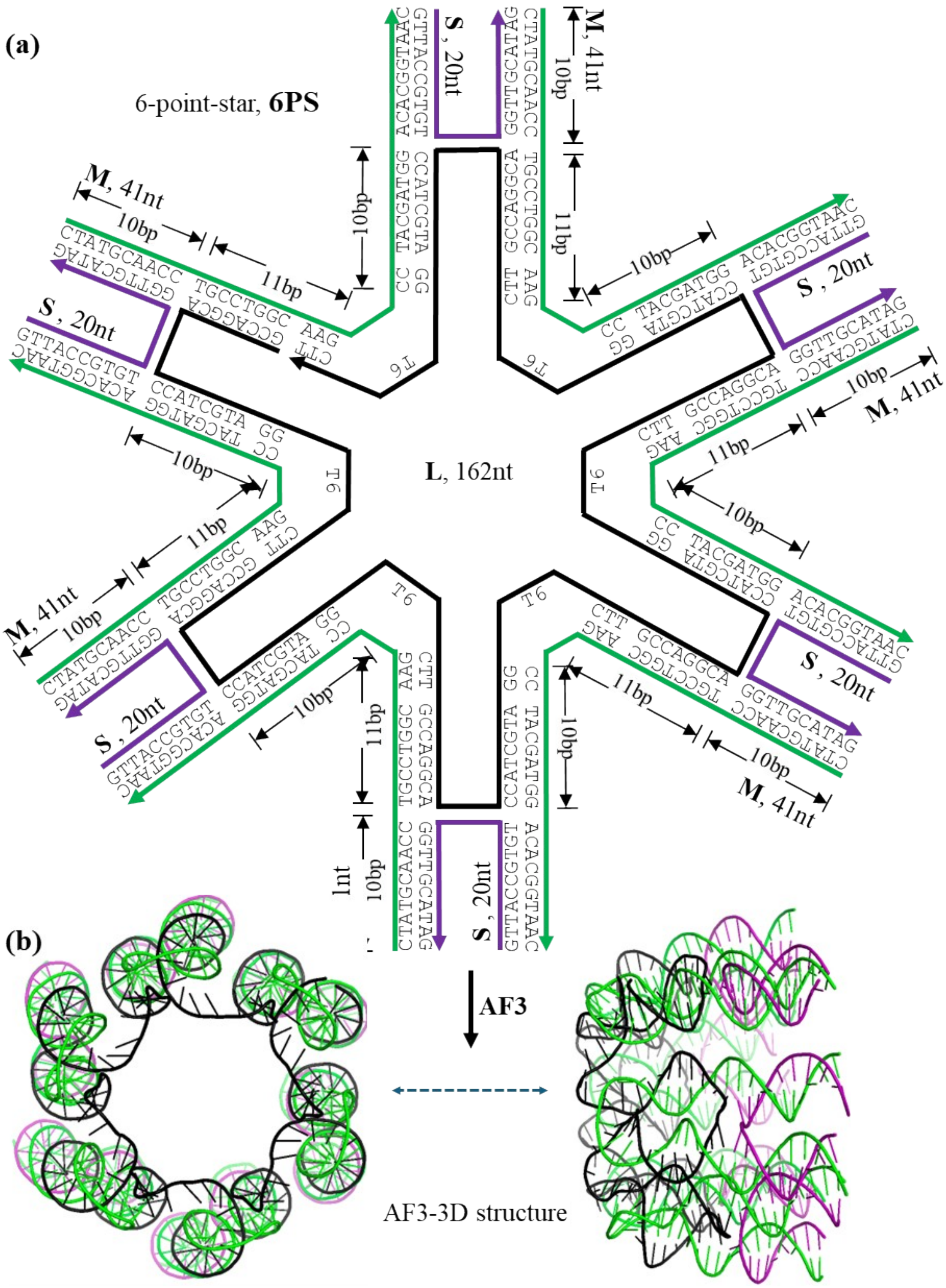
6-point-star, **6PS**
L, 162nt
M, 41nt
S, 20nt
10bp
11bp
1nt
T6
AF3
AF3-3D structure

continue…

(c)

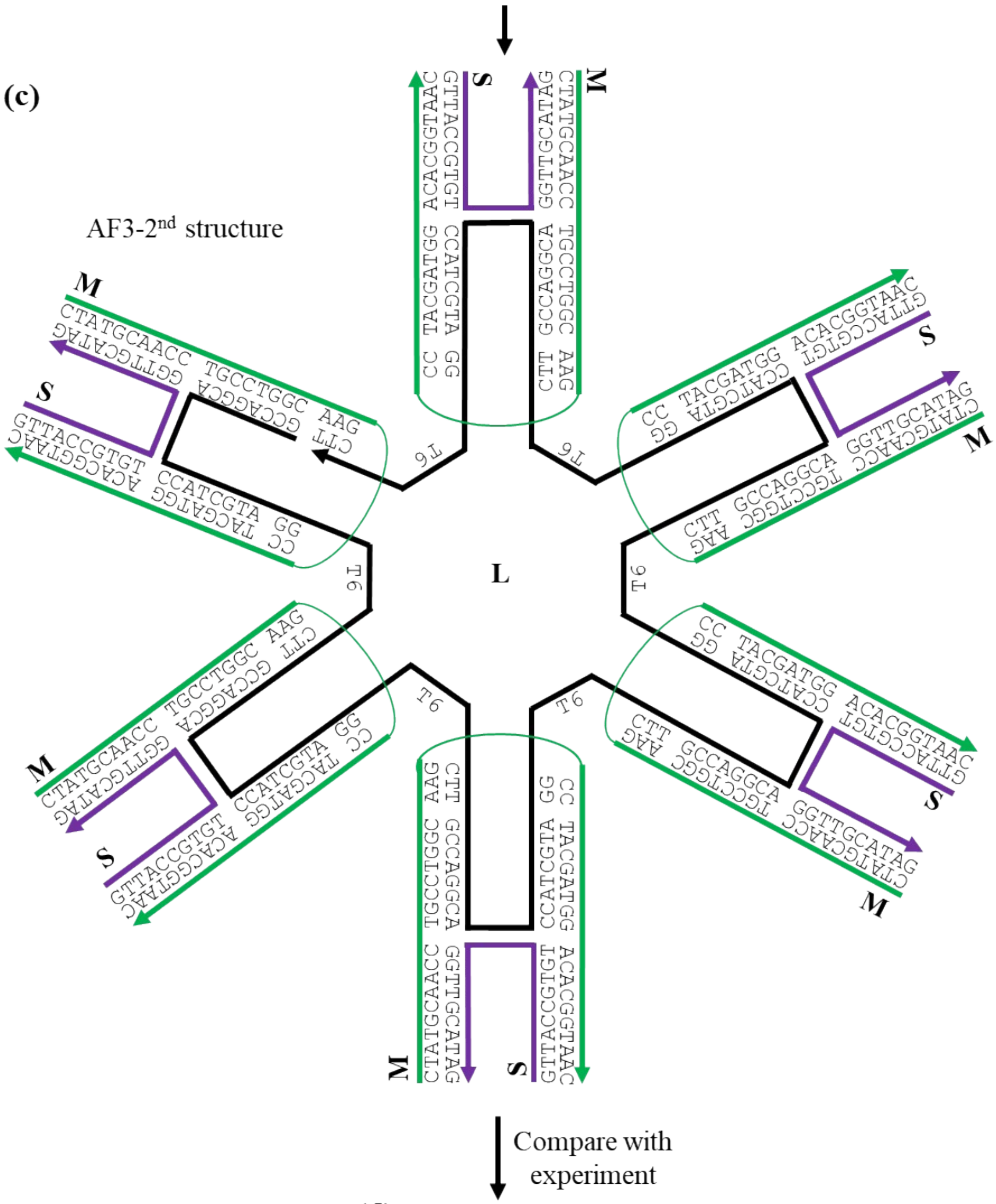

(d) **Inconsistent**

Figure S22. AF3 modeling of a symmetric DNA 6-point-star motif, s6PS. (a) The sequence design of the s6PS. Note that there is a 6-fold rotational symmetry at the motif center. All green strands are identical to each other and all red strands are identical to each other. (b) AF3-predicted 3D model of the s6PS in two orthogonal views. (c) The corresponding secondary (2nd) structure of the 3D structure. *Note that the green strands make U-turns in the same branch instead of crossing from one branch to another branch at the motif center*. (d) Comparison between the AF3 model and experimentally observed 2nd structure.

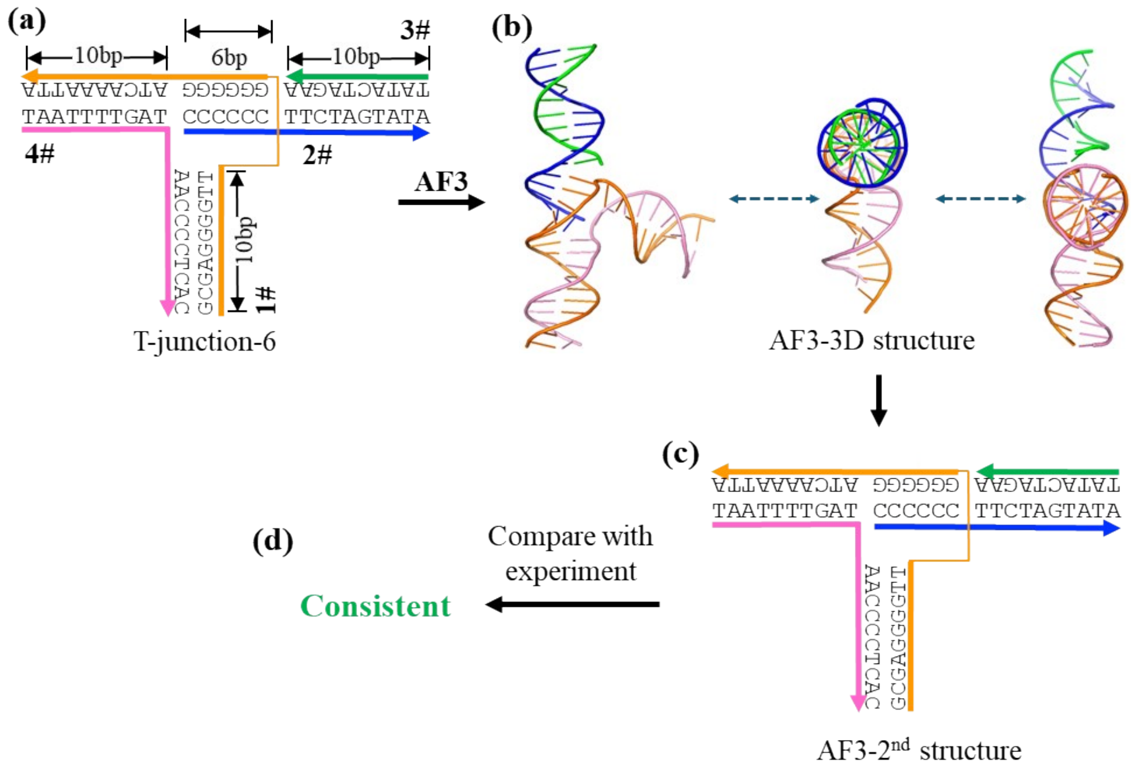

Figure S23. AF3 modeling of a DNA T-junction motif. (a) The sequence design of the T-junction. (b) AF3-predicted 3D model of the T-junction in three orthogonal views. (c) The corresponding secondary (2nd) structure of the 3D structure. (d) Comparison between the AF3 model and experimentally observed 2nd structure.

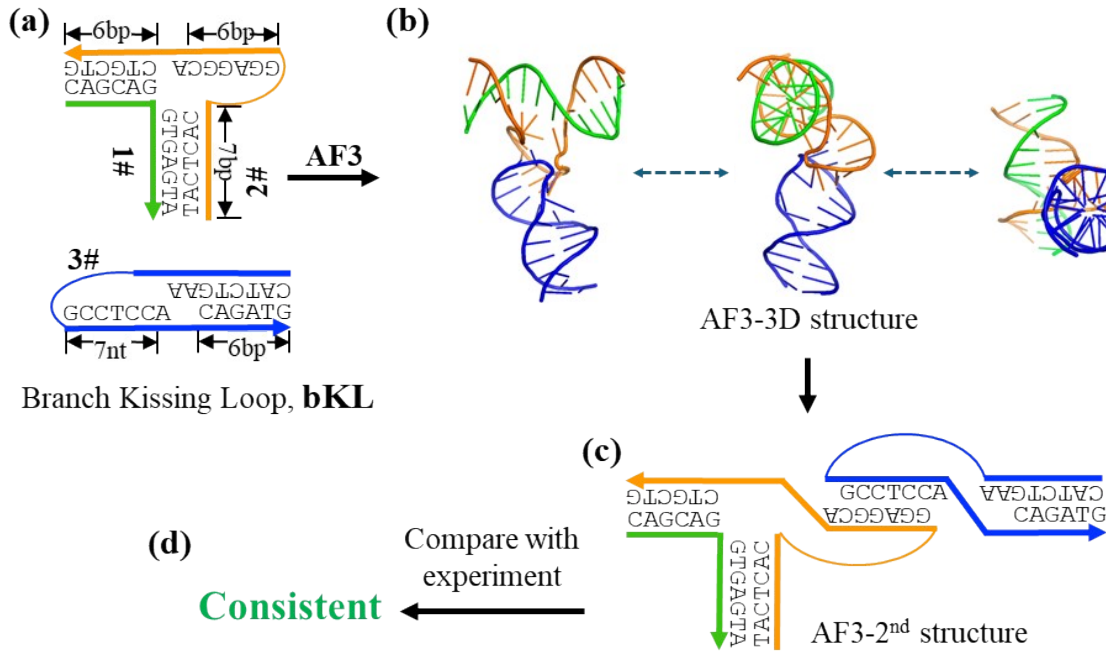

Figure S24. AF3 modeling of a DNA branch kissing loop, bKL. (a) The sequence design of the bKL. (b) AF3-predicted 3D model of the bKL in three orthogonal views. (c) The corresponding secondary (2nd) structure of the 3D structure. (d) Comparison between the AF3 model and experimentally observed 2nd structure.

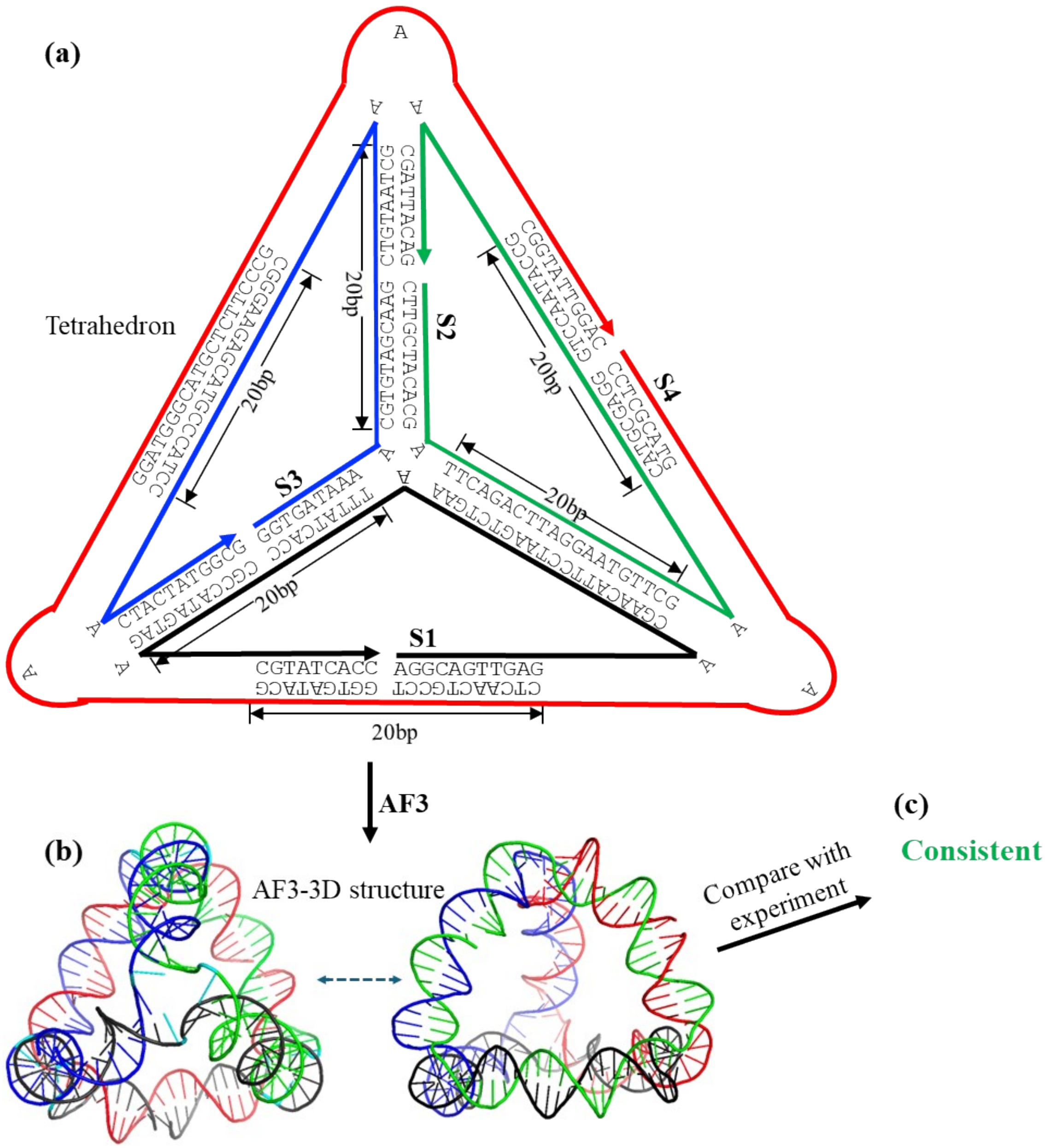

Figure S25. AF3 modeling of a DNA tetrahedron. (a) The sequence design of the tetrahedron. (b) AF3-predicted 3D model of the tetrahedron in two orthogonal views. (c) Comparison between the AF3 model and experimentally observed 2[nd] structure.

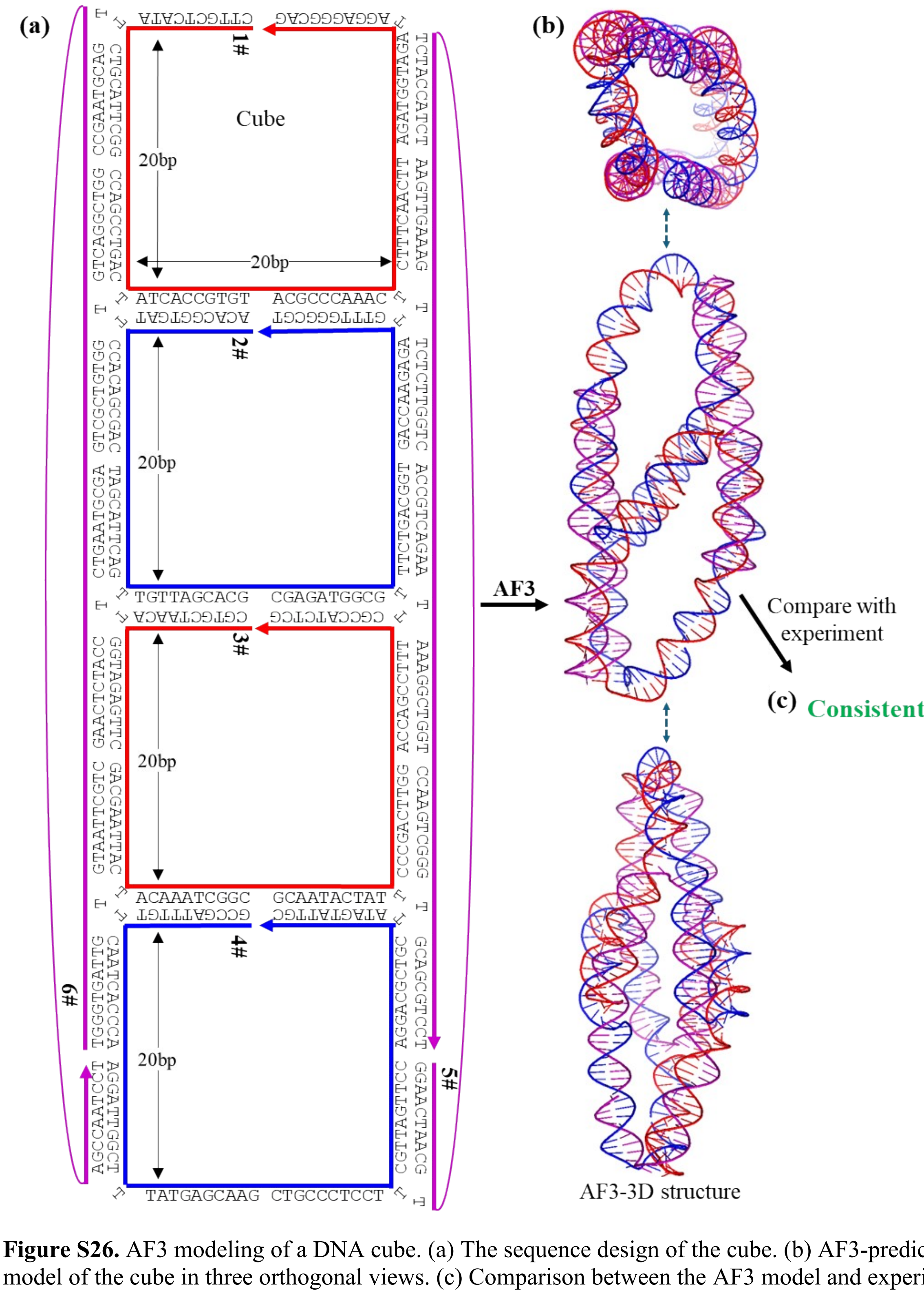

Figure S26. AF3 modeling of a DNA cube. (a) The sequence design of the cube. (b) AF3-predicted 3D model of the cube in three orthogonal views. (c) Comparison between the AF3 model and experimentally observed 2nd structure.

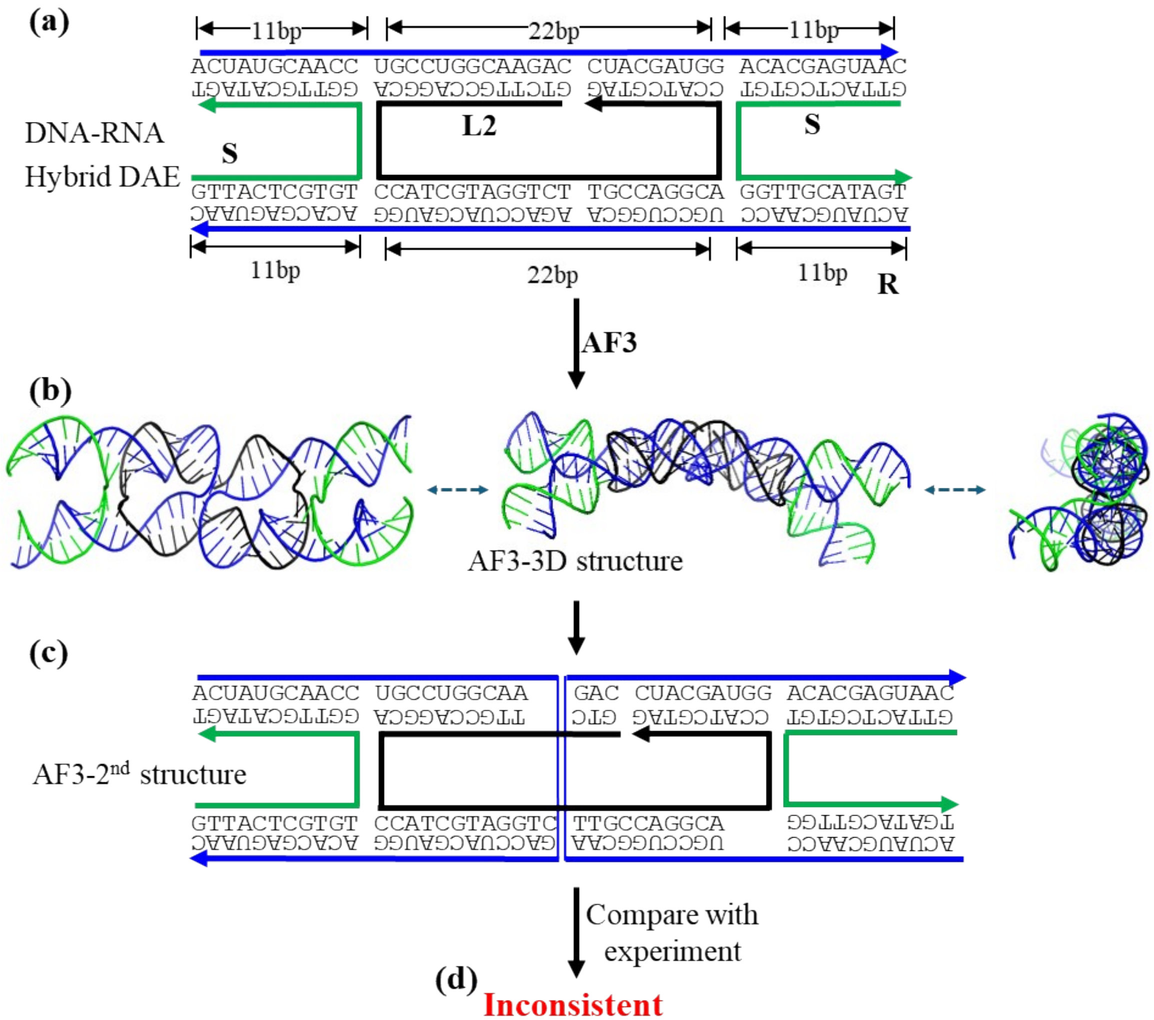

Figure S27. AF3 modeling of a DNA-RNA hybrid, antiparallel, double crossover, DNA-RNA DAE. (a) The sequence design of the DNA-RNA DAE. (b) AF3-predicted 3D model of the DNA-RNA DAE in three orthogonal views. (c) The corresponding secondary (2nd) structure of the 3D structure. *Note that the blue strands cross from one duplex to the other duplex instead of being continuous on one duplex.* (d) Comparison between the AF3 model and experimentally observed 2nd structure.

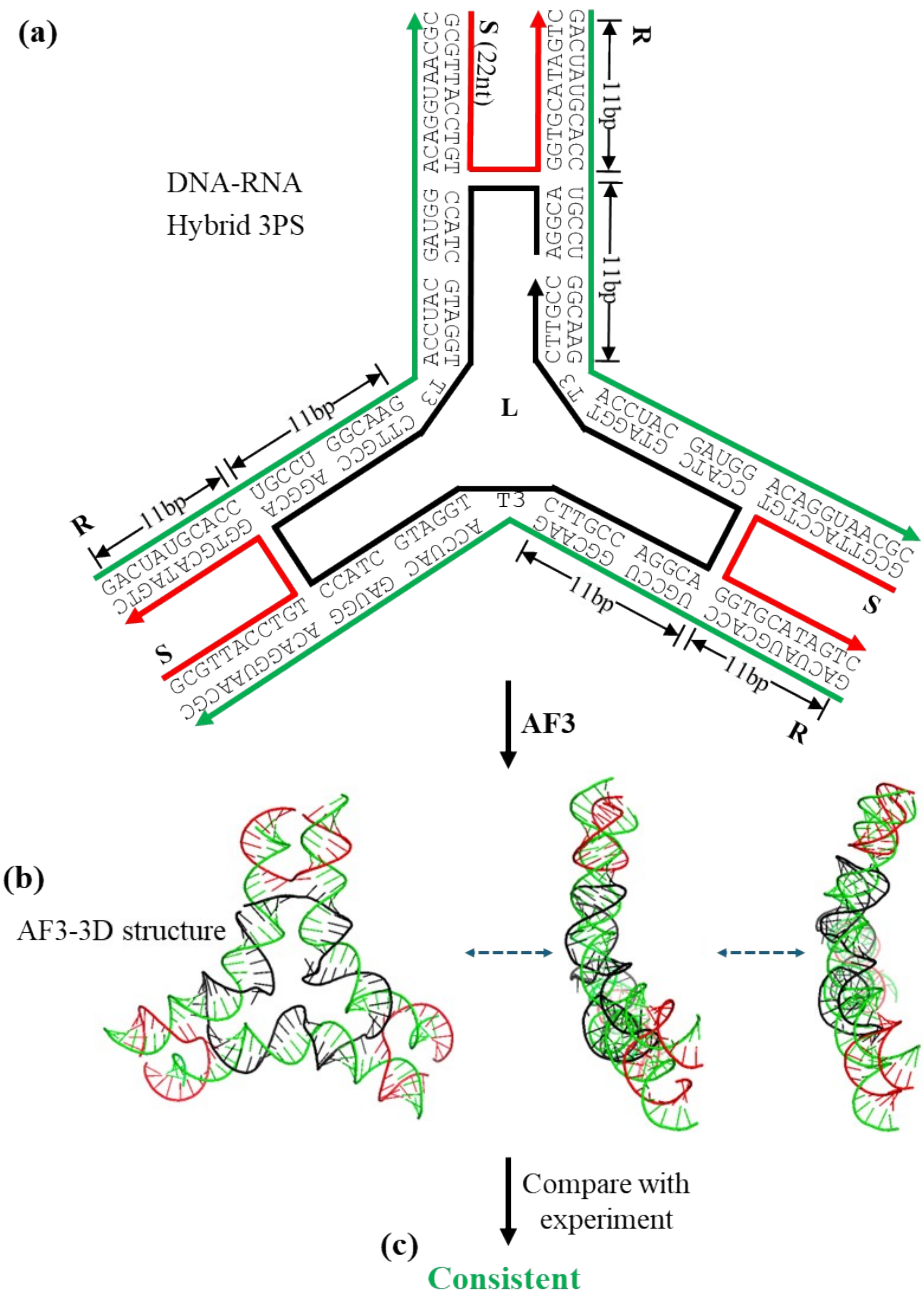

Figure S28. AF3 modeling of a DNA-RNA hybrid 3-point-star, DNA-RNA 3PS. (a) The sequence design of the DNA-RNA 3PS. (b) AF3-predicted 3D model of the DNA-RNA 3PS in three orthogonal views. (c) Comparison between the AF3 model and experimentally observed 2nd structure.

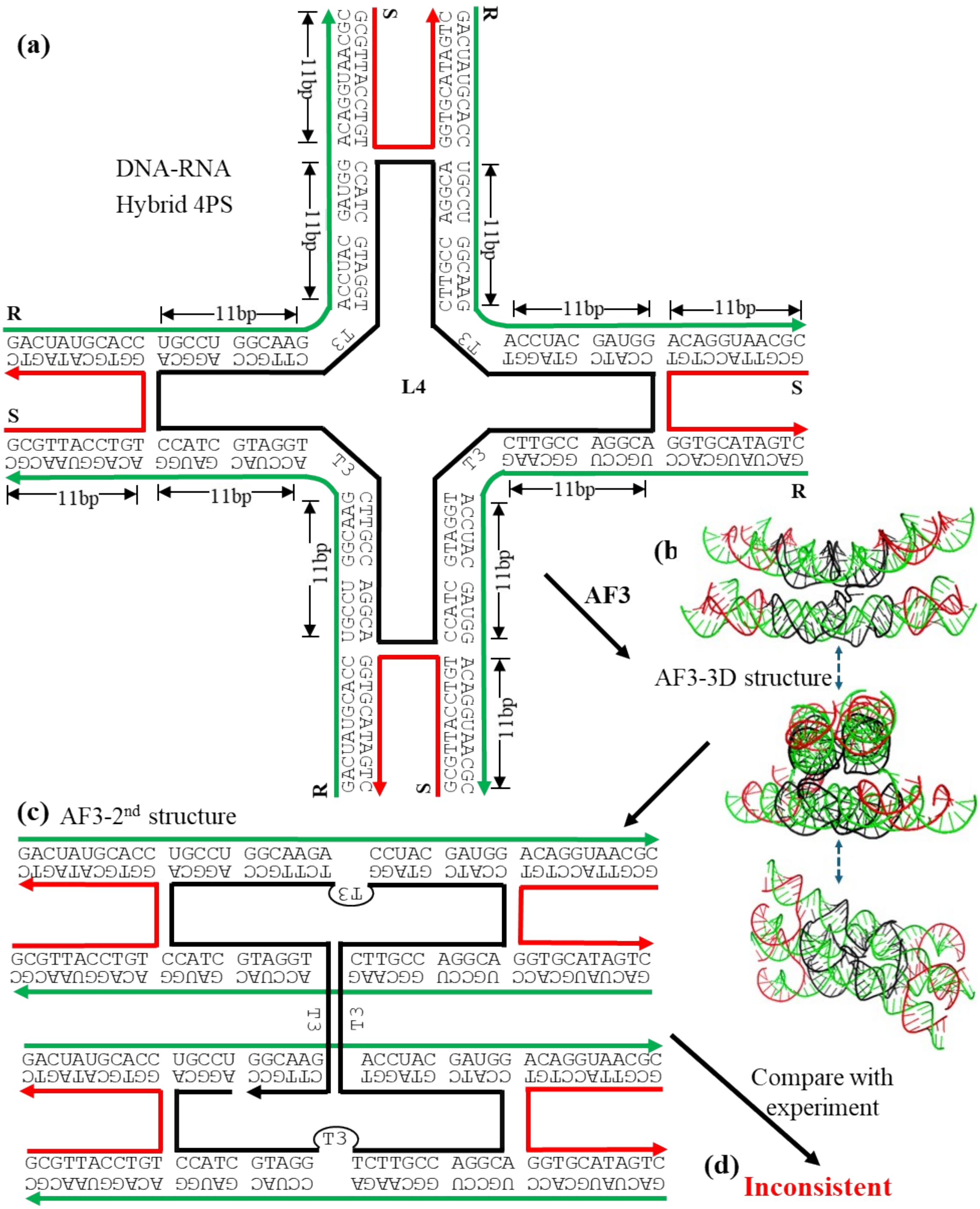

Figure S29. AF3 modeling of a symmetric DNA-RNA hybrid 4-point-star, DNA-RNA s4PS. (a) The sequence design of the DNA-RNA s4PS. (b) AF3-predicted 3D model of the DNA-RNA s4PS. (c) The corresponding secondary (2nd) structure of the 3D structure. *Note that the four branches stack onto each other into two pairs instead of being an open cross distribution.* (d) Comparison between the AF3 model and experimentally observed 2nd structure.

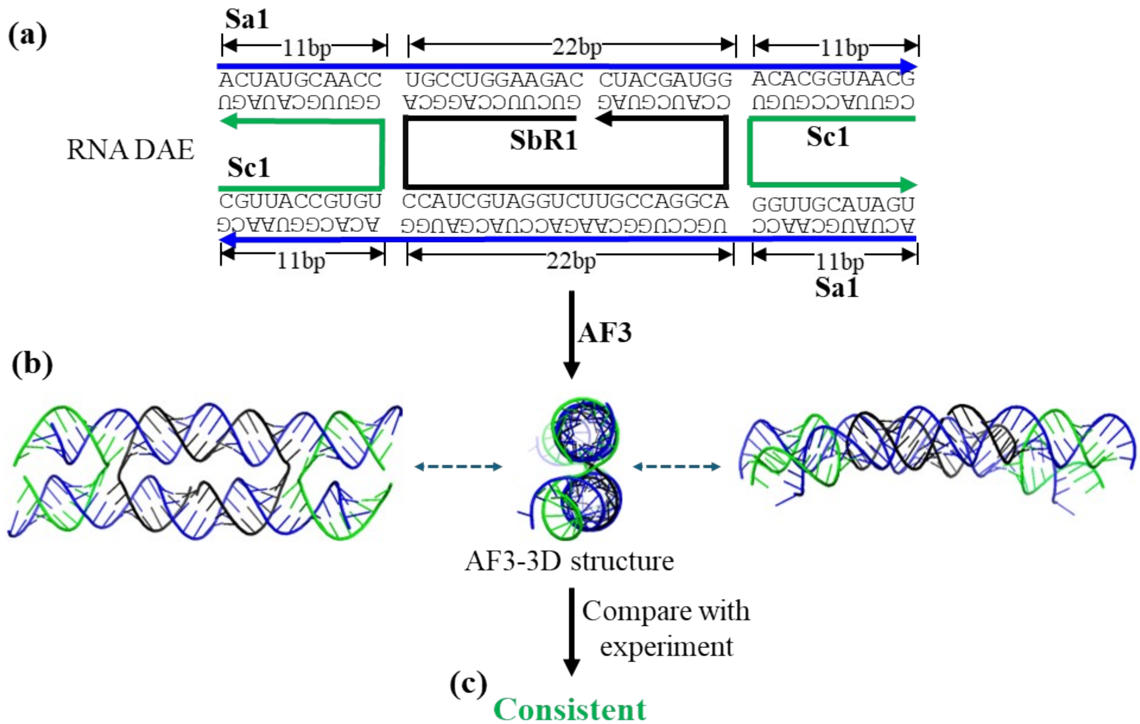

Figure S30. AF3 modeling of an RNA DAE. (a) The sequence design of the RNA DAE. (b) AF3-predicted 3D model of the RNA DAE in three orthogonal views. (c) Comparison between the AF3 model and experimentally observed 2nd structure.

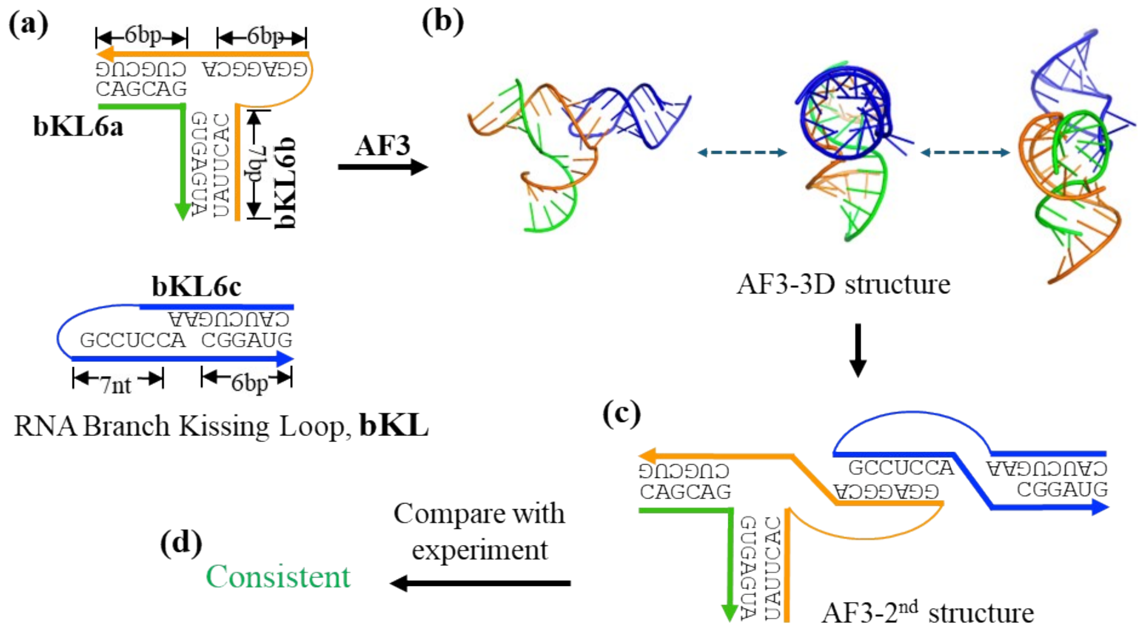

Figure S31. AF3 modeling of an RNA branch kissing loop, RNA bKL. (a) The sequence design of a the RNA bKL . (b) AF3-predicted 3D model of the RNA bKL in three orthogonal views. (c) The corresponding secondary (2nd) structure of the 3D structure. (d) Comparison between the AF3 model and experimentally observed 2nd structure.